8

MECHANICAL PROPERTIES OF NANOGLASSES

8.1 INTRODUCTION

Bulk metallic glasses (BMGs) combine unique mechanical properties, such as high strength and hardness with substantial fracture toughness [19, 18, 144, 7], but usually exhibit negligible global plasticity under uniaxial tension [145]. If loaded in a state of uniaxial stress, BMGs fail catastrophically along a single or a small number of shear bands [39]. For improving the plasticity under tension, pre-deformed samples and glasses with nanocrystalline inclusions have been studied in the past. It was found that an inhomogeneous microstructure with crystalline dendrites in an amorphous matrix stabilizes the glass against catastrophic failure and increases the ductility by developing a highly organized pattern of multiple shear bands distributed uniformly throughout the BMG [146, 39, 40, 41, 36]. Pre-deformation, like cold rolling, leads to a pseudo-composite structure consisting of a softer phase inside pre-induced shear bands (SBs) and a harder phase in the undeformed regions [33, 37, 38]. Generally speaking, these microstructural features improve the macroscopic plasticity by promoting the nucleation of secondary shear bands and shear band branching, as well as by limiting shear band propagation due to the intersection of shear bands. Therefore, it is an interesting question, if nanoglasses (NGs) with microstructural inhomogeneities exhibit improved plasticity. If a metallic NG contains interfaces, which exhibit structural features comparable to shear bands, we expect to observe enhanced plasticity like in the case of pre-deformed metallic glasses.

Within theses interfaces not only the topology but also the composition can be different from the bulk glass. In a previous chapter we showed that in the case of amorphous CuZr alloys, Cu-atoms segregate to the surface at elevated temperatures [137, 138, 139]. When consolidating a glassy nanopowder, which has been subjected to a pre-annealing process, a NG characterized by interfaces with an increased Cu–concentration should form. Therefore, another question is how these interfaces with Cu-segregation influence the mechanical behavior of a NG.

8.2 RESULTS AND DISCUSSIONS

In this study we investigate the mechanical properties of $Cu_{64}Zr_{36}$ NG under tensile load and compare to the case of a homogeneous bulk glass. A systematic investigation of the deformation mechanism of NG by varying the grains size and geometry is also conducted.

8.2.1 *Nanoglass with columnar grains*

In the first set of simulations we study the case of a NG free of pores, namely by consolidating columnar grains with a hexagonal cross section. Two types of NGs with the same geometry and same number of atoms ($\approx 5.5{\cdot}10^5$) were generated by compacting 18 glassy grains. In one case a chemically homogeneous glassy powder is used. In the other case a glassy powder with Cu–atoms segregated to the surfaces, which was generated by pre-annealing a glassy particle at 800 K (about 0.85 T_g) for 10 ns. Both metallic glass powders, with and without surface segregation, are compacted by applying an external hydrostatic pressure of 3 GPa at 50 K to obtain a NG free of pores.

For studying the deformation mechanism of NGs in comparison to a homogeneous BMG ($\approx 1.3{\cdot}10^6$ atoms), the structures have been deformed under uniaxial tension parallel to the z-direction. All structures were deformed at 50 K with a constant strain rate of $4\times10^7\ 1/s$ in z-direction. Periodic boundary conditions were applied in all three dimensions and the pressure in x- and y-direction was adjusted to 0 kbar allowing for lateral contraction. The stress-strain curves for both NGs and the BMG under tensile deformation are plotted in Fig. 29(a). Up to a strain of about 2%, all three curves show a similar slope and, thus, the interfaces have no strong influence on the elastic deformation. The stress at which the curves deviate from a linear behavior is defined to be the yield stress of the samples, which is significantly lower for both NGs at about 2.4 GPa compared to the bulk glass with a yield stress of approximately 3.3 GPa. The same trend is found for the maximum stress, which is 3.9 GPa for the inhomogeneous NG and 4.0 GPa for the homogeneous NG compared to 4.7 GPa in the case of the BMG. This can be explained by the lower activation barrier for shear transformation zones (STZs) in the NG interfaces due to a lower population of FI compared to the bulk glass. Cu-centered full icosahedra are VPs with a high packing density [88] and high shear resistance [59] and, therefore, those regions in a glass with a lower content of FIs are easier to deform plastically. This result is supported by an analysis of the atomic scale mechanisms during deformation. The local atomic shear strain [103] has been calculated with the OVITO analysis and visualization software [104]. Up to a strain of 8%, where the maximum stress is reached, STZs are only activated in the soft interface regions (see Fig. 30). With increasing strain, in both NGs, multiple embryonic shear bands are formed along the interfaces and eventually

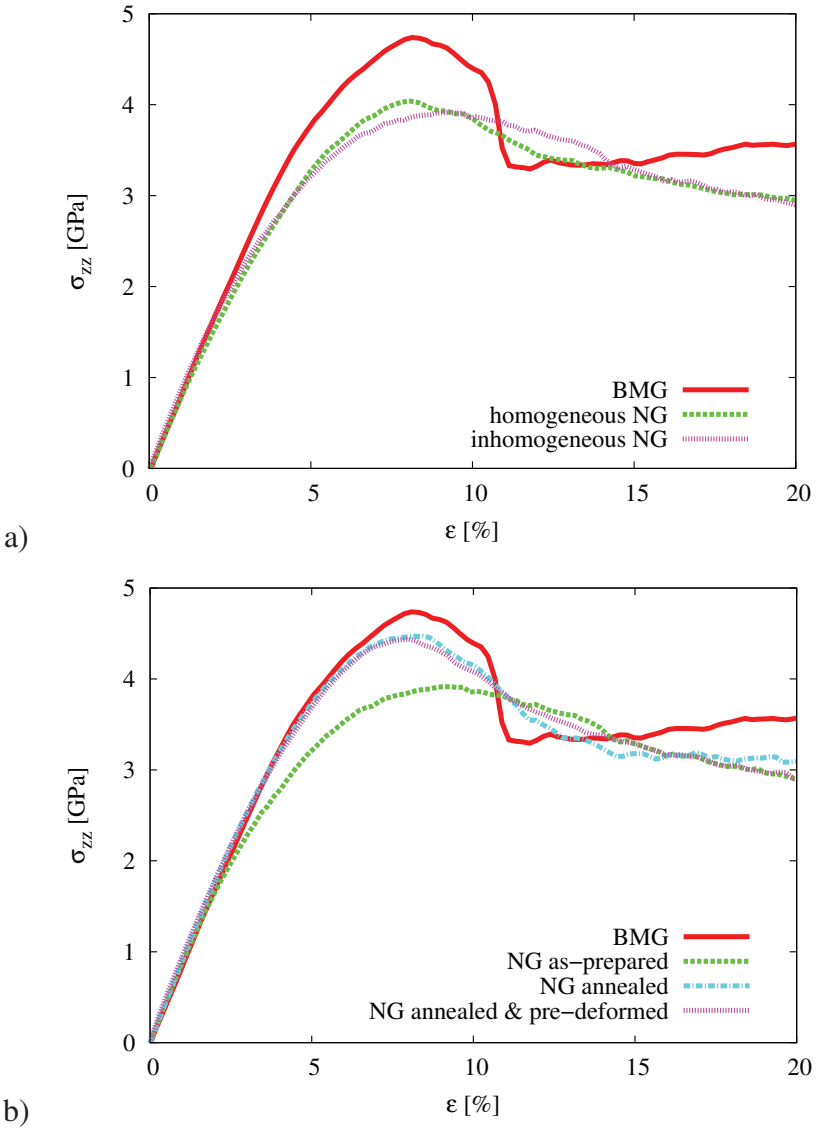

Figure 29: Tensile stress-strain curves at 50 K for: a) BMG, and as-prepared homogeneous (with homogeneous elements distribution) and inhomogeneous (with Cu-enriched interfaces) nanoglasses; b) BMG, as-prepared, annealed, annealed and pre-deformed inhomogeneous nanoglass, at a constant strain rate of $4\times10^{7}\ 1/s$.

start to propagate through the grain interiors. Due to the high number of embryonic shear bands formed in the interfaces, the elastic energy is released homogeneously in the entire sample. Since shear band propagation is driven by the elastic energy [99], the local energy release is not sufficient to accelerate one of the shear bands, so that is goes critical. Consequently, both NGs deform homogeneously in contrast to the BMG, which exhibits localized deformation in one major shear band (see Fig. 30, top). The propagation of one single shear band leads to a significant stress drop in the case of the BMG, which is not observed for the NGs due to the branching into multiple shear bands leading to a more homogeneous deformation. For larger strains the homogeneous sample and the annealed NG show a slight increase in flow stress, which is due to the fact the shear bands have to rotate in the 3-dim. periodic setup and the Schmid factor is decreasing. The flow strain of the as-prepared sample, however, is similar to the annealed and predeformed one. In these cases, we observe a strain softening at larger strains, because plastic flow occurs more homogeneously in a network of interpenetrating shear bands.

Besides the homogeneously released elastic energy, shear band propagation is compromised by the intersection of shear bands with different orientation (see Fig. 30). This effect has already been observed in metallic glasses that were pre-deformed by cold rolling [38].

A quantitative interpretation of strain localization has been realized by using the parameter ψ for describing the degree of strain localization defined by Cheng *et al.* [60],

$$\psi = \sqrt{\frac{1}{N}\sum_{i=1}^{N}(\eta_i^{Mises} - \eta_{ave}^{Mises})^2}. \tag{8.1}$$

A larger ψ value indicates larger fluctuations in the atomic strain and a more localized deformation mode. Comparing the strain localization parameters for the NGs and BMG (see Fig. 31) at a strain of 16 %, our observation of a more homogeneous deformation in the NGs is supported. Moreover, the values for both types of NGs are almost identical indicating that the Cu-segregation to the interfaces does not have a significant influence on the deformation behavior. We have shown in section 6.5.2 that glass-glass interfaces annealed at a temperature close to T_g are subject to a structural relaxation, involving a partial recovery of the icosahedral SRO. Still, the interface structure after annealing is characterized by a difference in the icosahedral SRO of about 2 % in comparison to the bulk. These results are in line with experimental observations on pre-induced shear bands produced by indentation [42] or cold rolling [133], where structural disorder is retained in the shear bands even after annealing without strongly affecting the mechanical behavior. Therefore, the question arises how thermal annealing prior to deformation does affect the plastic deformation mechanisms operating in a NG. In order to answer this question, both types of NGs have been subjected to an annealing process at 700 K (0.75 T_g) for 2 ns.

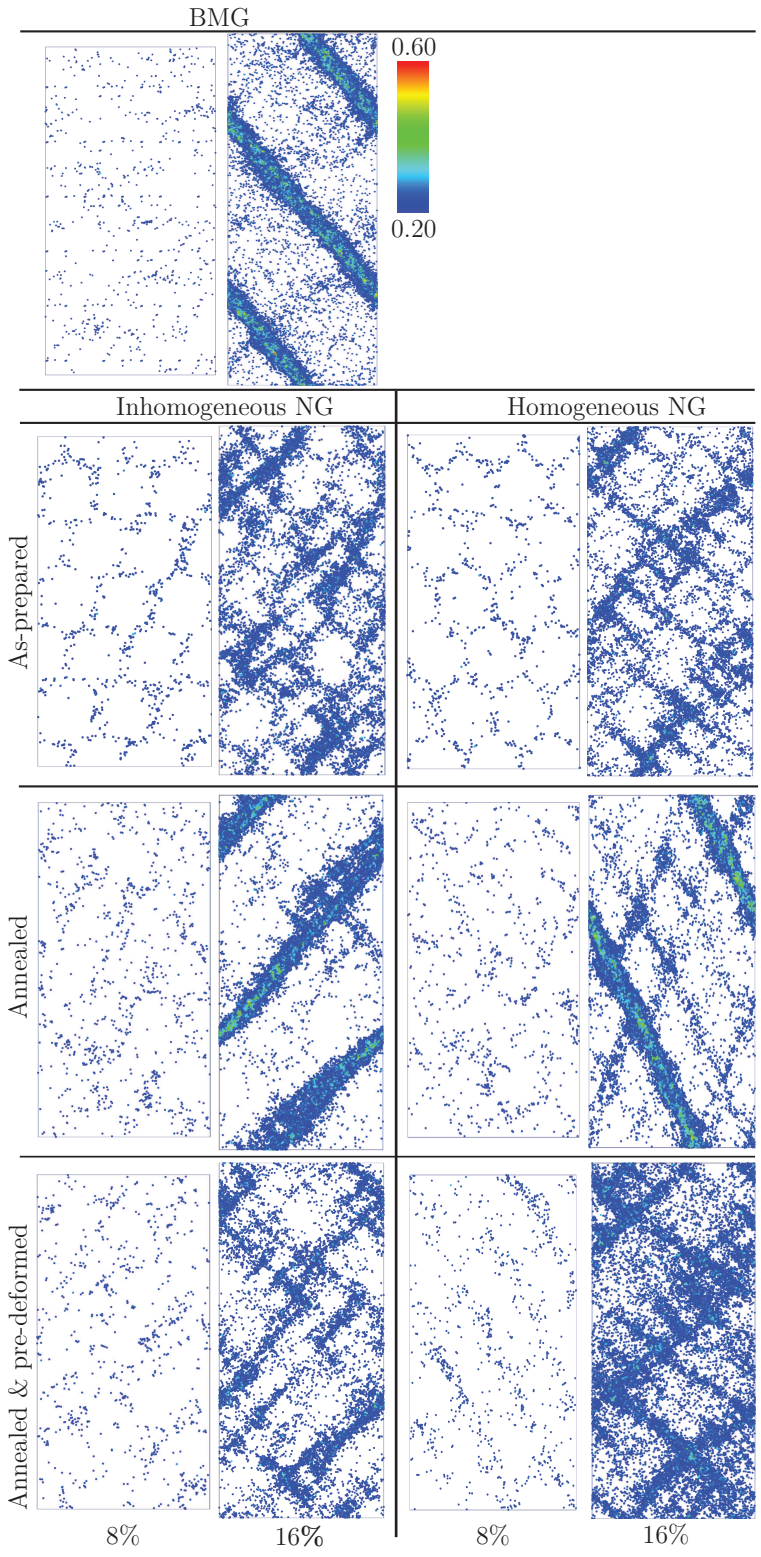

Figure 30: Local atomic shear strain for a inhomogeneous (with Cu-enriched interfaces) and homogeneous (with homogeneous elements distribution) nanoglasses as-prepared, annealed, annealed and pre-deformed in comparison with a BMG, under tensile deformation at 50K.

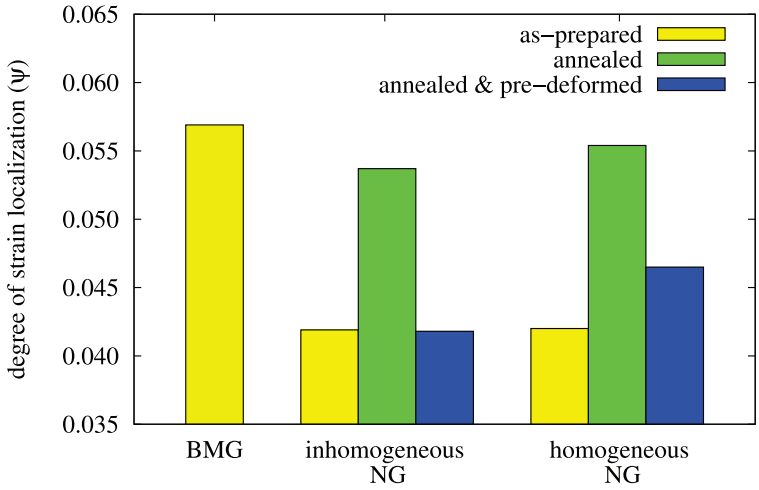

Figure 31: The ψ values for BMG, inhomegeneous and homegeneous nanoglasses, as-prepared, annealed, annealed and pre-deformed after plastic deformation to an overall strain of 16%.

After annealing the NGs have been cooled down to 50 K and subsequently deformed in uniaxial tension following the same procedure as before.

At a strain of 8 % shear transformations occur in the interfaces similar to the previous case of non-annealed NGs. When the strain is increased, however, the deformation mechanism changes. In agreement to experimental observations [133] the plastic deformation no longer takes place in a network of multiple shear bands. Instead, the deformation is more localized and at a strain of about 16 % one dominant shear band is formed. Nevertheless, the plastic deformation mechanism of the annealed NGs deviates from what has been observed for the BMG. The shear band in the annealed NGs is not as well localized as in the BMG. At a strain of 16 % even indications of shear band branching are observed (see Fig. 30), a mechanism which has been reported for BMGs with pre-induced SBs as well [33]. The same effect is also seen in the ψ-parameter, where the values of the annealed samples are higher than for the as-prepared NGs but not higher as for BMG (see Fig. 31). However, the SRO recovery in the interfaces is slightly more pronounced for the homogeneous NG, which results in a higher ψ-parameter, and therefore a more localized deformation. Moreover, comparing the stress-strain behavior for the BMG and the annealed NGs (see Fig. 29(b)), the differences are still significant. Therefore the interfaces in the annealed NGs still can have an impact on plastic deformation.

The next question we address is whether a homogeneous deformation mode can be recovered after annealing. Therefore the annealed NGs have been pre-loaded to a strain level of 8%, just where the plastic deformation already starts to initiate in the interfaces, but no localized shear bands occurs (see Fig. 30). After unloading to zero strain, the NGs were deformed for a second time. Interestingly, the plastic

deformation behavior is almost identical to that before annealing. The NGs undergo plastic deformation mediated by multiple shear bands, uniformly distributed over the sample volume. This is attributed to STZs which affect the short range order and, at a strain of 0.08, occur mainly in the soft interfaces. This is in good agreement with the ψ-parameters, which nearly shift back to the same values as found for as-prepared NGs. Again, the value for the homogeneous NG is higher indicating stronger shear localization. Consequently, the SRO in the interfaces, which had been recovered during annealing, is damaged during pre-loading and, again, the interfaces act as nucleation sites for shear bands preventing the plastic deformation to localize in a single shear band as in the case of BMGs or annealed NGs. Analyzing the stress-strain behavior of the different NGs upon tensile deformation (see Fig. 29(b)), we find the annealing process to increase the yield stress as well as the maximum stress. This is due to the recovery of interfacial SRO upon annealing, which leads to an increase in activation barriers for STZs in interfaces. Interestingly, the annealed and then preloaded NG shows an almost identical stress-strain behavior as the annealed NG, despite the observed differences in deformation mode.

8.2.2 *Grain size effects*

In polycrystalline materials the strength can be increased by means of decreasing the grain size, because grains boundaries obstruct the motion of dislocations [147]. Therefore the question we address here is whether by varying the glassy particle size and therefore the volume fraction of interfaces, the plastic deformation of NGs changes, and moreover, the strength of a NG is affected. For studying the grain size effect on the mechanical properties we constructed three homogeneous NGs following the same procedure as in the previous section using glassy grains with diameters of 4 nm, 10 nm (used in the previous section) and 16 nm, respectively. In the first case we used 91 glassy nanoparticles for NG compaction while for the large grains we used 18 nanoparticles. The total number of atoms was $\approx 8.0{\cdot}10^5$ and $\approx 2.0{\cdot}10^6$, respectively.

For studying the plastic behavior all three NGs were deformed in tension following the same procedure as described before. The stress-strain curves of all three NGs and the BMG under tensile deformation are plotted in Fig. 32(b). Up to a strain of about 2% all four curves show a similar slope and, thus, the interfaces fraction has no strong influence on the elastic deformation. In contrast the yield stress and maximum stress decrease considerably with decreasing grain size resulting in a work softening. This result is contradictory to the case of polycrystalline materials where an increase in the grain boundary fraction induces work hardening. The difference can be explained by the deformation mechanisms for nanocrystalline structures and NGs, respectively. If in polycrystalline materials grain boundaries act as sources and sinks for dislocations, in contrast, the interface soft regions in NGs act as sources for embryonic shear bands.

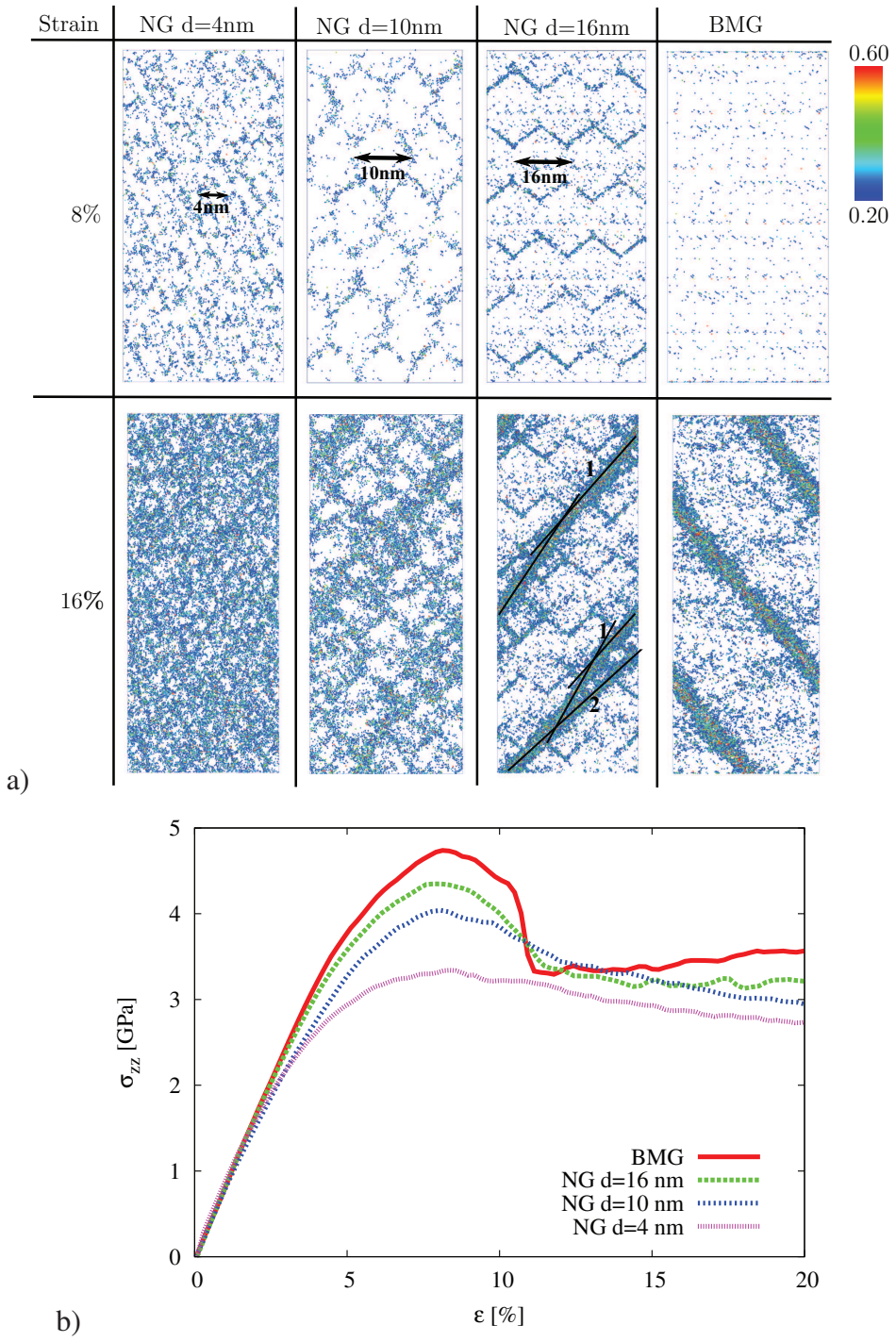

Figure 32: a) Local atomic shear strain for NGs with grain size of 4 nm, 10 nm and 16 nm in comparison with a BMG under tensile defromation at 50K, b) and the corresponding tensile stress-strain curves at 50 K at a constant strain rate of $4\times10^7\ 1/s$.

An increased number of interfaces results in a soft NG. On the other hand, an increase of the volume fraction of interfaces in a NG shows an improved plastic behavior. As was shown in the previous section a large number of interfaces cause a homogeneous deformation of the NG. In order to check our prediction we also calculated the local atomic shear strain for each of these NGs in comparison to the case of the BMG. Up to a strain of 8% in all three NGs, STZs are mostly activated in the soft interface regions as it was already expected based on the previous results (see Fig. 32(a)). Moreover, in case of the NG with the largest grain size the STZs are activated in the interfaces oriented close to a 45°-angle but not in the interfaces oriented perpendicular to the loading direction.

Although the shear band nucleation process is similar in all three NGs, the shear band propagation strongly differs in case of NG with the largest grain size in comparison to the other two NGs. It can bee seen in Fig. 32(a) that the plastic deformation is more localized at a strain of 16%, in case of the NG with a grain size of 16 nm. This can be explained by the low fraction of soft interfaces with respect to the NG volume. Due to the low number of embryonic shear bands formed in the interfaces, the elastic energy is not released homogeneously in the whole NG. Instead, the deformation is more localized but still far from the well localized deformation in the BMG. At a strain of 16% indications of shear band blocking are observed. In Fig. 32(a) two major shear bands are identified initially oriented in a 45°-angle with respect to the tensile axis. When the first shear band intersects an interface, the propagation direction is slightly modified. Therefore the shear bands are not parallel anymore, will intersect, and block each other. The involved sample is too small to study in detail shear bands blocking, but we can predict based on previous result that macro-scale deformation is also homogeneous even in a NG constructed by compacting glassy nanoparticles with larger sizes. Here shear bands block each other preventing catastrophic failure along a single or small number of shear bands.

8.2.3 *Nanoglass with spherical grains*

In the previous section we presented results on the influence of interfaces on the mechanical properties of NGs free of pores, comprising columnar glassy grains with a hexagonal cross section. The last question we address is whether the presence of pores can also have an impact on the mechanical properties of a NG. In section 7.1 we showed that constructing NGs using a glassy nanopowder with a spherical geometry resulted in a structure that is characterized by interfaces and also pores. Therefore a NG with an idealized microstructure was constructed by consolidating glassy spheres of 10 nm diameter starting from an initially face centered cubic arrangement. The spherical powder was annealed at 800 K for 10 ns prior compaction and Cu-atoms segregated to the surfaces. The NG was compacted following the same procedure as in the case of NGs with columnar grains. The NG has a total number of atoms of about

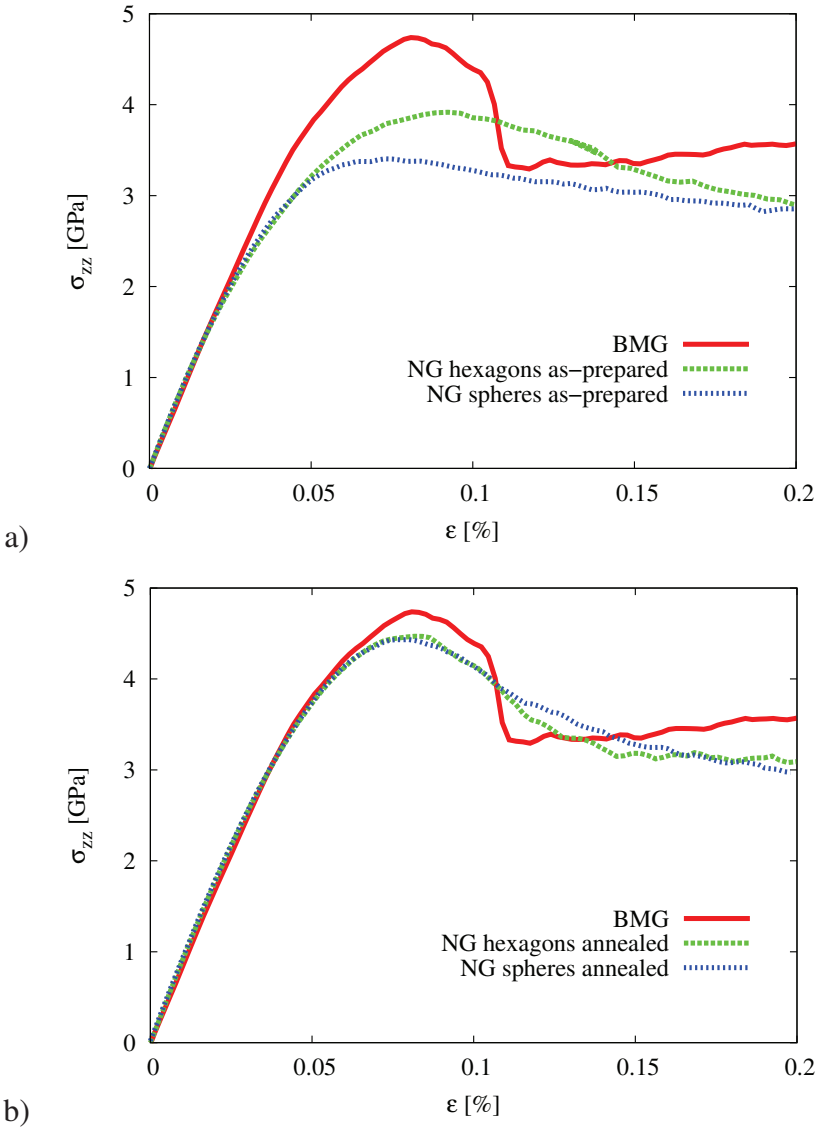

Figure 33: Tensile stress-strain curves at 50 K for: a) BMG, and as-prepared nanoglasses with columnar and spherical glassy grains; b) BMG and annealed nanoglasses with columnar and spherical glassy grains, respectively, at a constant strain rate of $4\times10^7\ 1/s$.

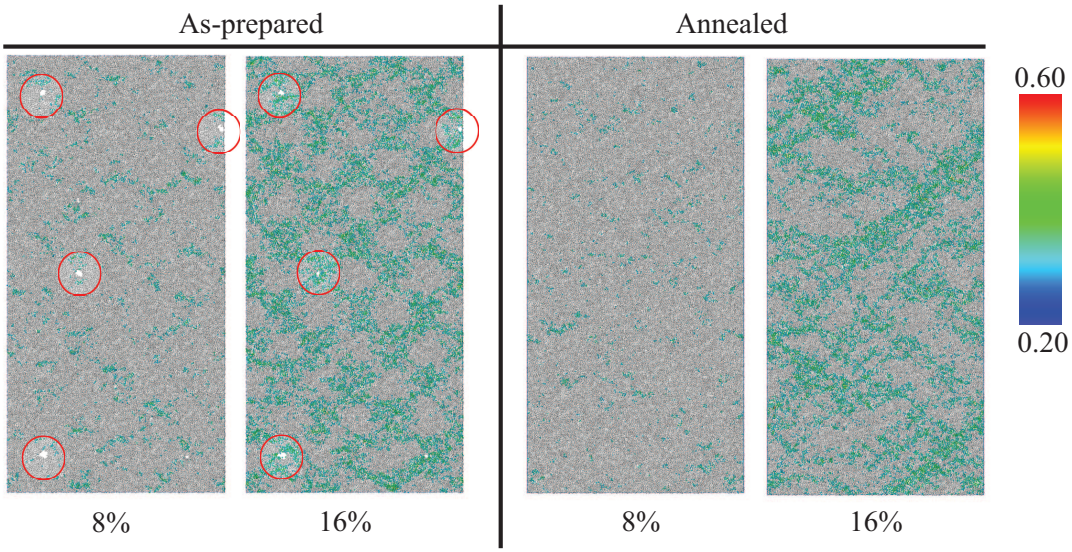

Figure 34: Local atomic shear strain for inhomogeneous (with Cu-enriched interfaces) nanoglasses as-prepared, and annealed under tensile deformation at 50K. The red circles show the pores from the as-prepared nanoglass.

10^6. After compaction a NG characterized by interfaces with enhanced Cu-atoms and also pores is obtained. The pores diameters range between 1-3 nm. For studying the deformation mechanism of this NG in comparison to the previous type of NG free of pores and a homogeneous BMG, the structure has been deformed following the same procedure as in the previous section. Both types of NGs studied (with spherical and columnar grains) are inhomogeneous (with Cu-enriched interfaces).

The stress-strain curves for the NGs with spherical and columnar grains and BMG are plotted in Fig. 33(a). Again, up to a strain of about 2%, all three curves show a similar slope, which means that the pores have no strong influence on the elastic deformation. On the other hand, the maximum stress of the NG with pores is approximately 3.4 GPa, which is lower compared to 3.9 GPa in the case of NG free of pores. The presence of the pores can serve as an explanation for a lower maximum stress. Moreover, a lower value of maximum stress can be explained by a higher volume fraction of interfaces in the NG with pores. The model used for generating the NG microstructures with spherical grains serve as an explanation.

Analyzing the local atomic shear strain of the NG with pores we found that these pores do not serve as sources for formation of embryonic shear bands. Again, as in the case of the NG free of pores at a strain of 8% the STZs are activated mostly in the interface regions (see Fig. 34). Around the pores (see red circle) there is almost no local atomic shear strain. This suggests that the activation barrier for STZs is lower in the soft interfaces when compared to the regions around the pores. Further deformation of the NG to a strain of 16% leads to a decreasing pore size. This is due

to the tensile deformation which biases structural rearrangements by facilitating flow [148]. Moreover, also the NG with pores deforms more homogeneously due to the high number of embryonic shear bands formed in the interfaces.

Finally, we study whether these pores are stable under thermal treatment. Annealing the NG at 700 K for 5 ns, we found that the pores vanish completely and, the resulting annealed structure is free of pores (see Fig. 34). The annealed NG is further deformed, as described before. In Fig. 33(b) stress-strain curves for annealed NGs with spherical and columnar grains and BMG are shown. One can see that yield stress and maximum stress are almost the same values for both types of NGs. Interestingly, the plastic deformation of annealed NG with spherical grains is more homogeneous compared to the case of the annealed NG with columnar grains. It can be seen in Fig. 34 that at a strain of 16% no dominant shear band is formed. This can be explained by the higher volume fraction of interfaces in a NG obtained by compacting spherical glassy grains in comparison to the case of a NG with columnar grains. In addition, the free volume associated with the pores spreads into the NG under thermal treatment, increasing the fraction of local soft regions. An increase of the interfaces density in addition to the excess free volume resulted from dissolution of pores causes a more homogeneous plastic deformation in the annealed NG with spherical grains.

8.3 SUMMARY

In this study, we have investigated the plastic behavior of $Cu_{64}Zr_{36}$ NGs with microstructural inhomogeneities obtained by powder consolidation. These inhomogeneities or interfaces possess an atomic structure which deviates from the bulk and is characterized by an excess free volume or increased Cu-atoms density, lower SRO and increased potential energy. Under tensile deformation, the NGs exhibit a homogeneous plastic deformation in a highly organized pattern of multiple shear bands, distributed in the whole sample, in contrast to a BMG, where the plastic deformation is confined in one single shear band. We show that shear banding is preferentially initiated in the interfaces or soft regions, and these shear bands can distribute the applied strain more homogeneously. Moreover, the plasticity of a NG can be easily tuned by thermal treatment or prior-deformation. By increasing the grain size, and, therefore decreasing the number of soft interfaces we showed that the NG exhibits a more localized deformation. In addition, we found that the presence of pores in the NG has not a strong impact on the plastic deformation. Therefore, it can be anticipated that NGs exhibit an enhanced ductility as compared with BMG.

9

VIBRATIONAL PROPERTIES OF NANO-STRUCTURED MATERIALS

9.1 INTRODUCTION

Phonons generally affect the thermal, optical, mechanical and electrical properties of materials. While the phonon density of states (PDOS) is primarily a function of the local atomic structure, it is also sensitive to atomic level stresses and the microstructure. If the characteristic length scales get down to the nanometer regime, deviations of the PDOS from the corresponding bulk structure have been observed, both in experiment and theory [43, 44, 45, 46, 47, 149]. By conducting a study on the PDOS of nanoglasses, evidence for the existence of interfaces could potentially be found. Since the microscopic origins of the observed size-effects in case of different nanomaterials are very often not clear, a complete description of size effects on the PDOS of nanomaterials (free nanoparticles, nanocrystals and embedded nanoparticles) is also carried out.

Size effects due to the variation of the surface to volume ratio are expected to scale with $D^{-\alpha}$ ($\alpha \approx 1$) [48], where D describes the intrinsic structural length, like grain or particle diameter. Phonon confinement due to finite particle size [150] or quantum phenomena originating from the discreteness of electron states and band-gap variation with nanostructure size [151], both scale with D^{-2}. The presence of grain boundaries (GBs) [43, 46, 152] or surfaces [48] leads to a locally lower atomic density and higher structural disorder in comparison to the bulk material resulting in additional vibrational modes at low and high frequencies [47]. Confinement effects affect the optical modes at the Brillouin zone center ($q = 0$), since more phonons with $q \neq 0$ (away from Brillouin zone center) contribute to the PDOS and lead to a red shift in Raman spectra [150, 44, 153]. This has been reported for different nanomaterials like nanocrystals [44, 154, 153], nanoparticles embedded in glass [45, 155] or other nanostructures [156]. The red-shift observed in Raman spectra, however, has also been explained by tensile surfaces stresses [113], while the blue-shift has been attributed to compressive surface stresses (or pressure) [114]. This interpretation was supported by atomistic simulations [48] that revealed the influence of surface stresses on the

PDOS, resulting in a shift of the entire PDOS towards higher frequencies for the case of metals.

In view of the partially controversial interpretation of the PDOS of nanostructured materials, a detailed study revealing the role of the various size effects appears to be a worthwhile task. In this chapter, we calculate the PDOS separately for nanoparticles, nanocrystals, nanoparticles embedded in a glass and a nanoglass. We determine how the vibrational modes are affected by changes in the nanostructure as compared to crystalline and amorphous bulk materials. Moreover, we show how the PDOS changes with nanoparticle size through surface stress and confinement effects. Classical molecular dynamics (MD) simulations are carried out using the MD code PARCAS [95]. Germanium is chosen as a prototype of a covalently bonded material with crystalline and amorphous modifications. Tersoff's interatomic potential for germanium was used in this study to represent the interactions between the atoms [101]. This potential is known to reproduce the structural properties of the crystalline, liquid and amorphous states of germanium [111]. For comparison, some of the calculations were repeated using the Stillinger-Weber potential [157]. In addition, the PDOS for $Cu_{64}Zr_{36}$ nanoglass is calculated using Mendelev's embedded atom type potential [100].

9.2 RESULTS AND DISCUSSIONS

9.2.1 *Free Nanoparticles*

In the first set of calculations, free non-supported particles were studied, which for simplicity were created as spherical cuts of the bulk phase and relaxed at 50K temperature before the PDOS was analyzed. The result is shown in Fig. 35(a), where the PDOS of the single crystal is compared with the PDOS of nanoparticles with diamaters of 3.9 nm and 7.5 nm. Essentially, two major features can be observed, namely the broadening of the acoustical branch and a red-shift of the entire distribution which gets more pronounced as the particle size decreases. The enhancement of the acoustical modes at lower frequency can be directly attributed to the presence of weakly bonded surface atoms, characterized by a lower coordination.

By removing all atoms with a diamond-like configuration from the PDOS calculation through a common neighbor analysis (CNA) [158], it becomes obvious that additional acoustic modes are due to surface atoms (see Fig. 35b), only, while the presence of surface atoms also leads to a slight blue shift in the optical modes.

The atoms located in the inner part of the particle, in contrast, exhibit a clear red-shift over the entire phonon frequency range. Here, in principle surface stress or confinement effects could serve as an explanation [159, 131]. In order to discriminate between both, we have recalculated the PDOS using another interatomic potential for Ge, namely the Stillinger-Weber format. By construction, this potential has no

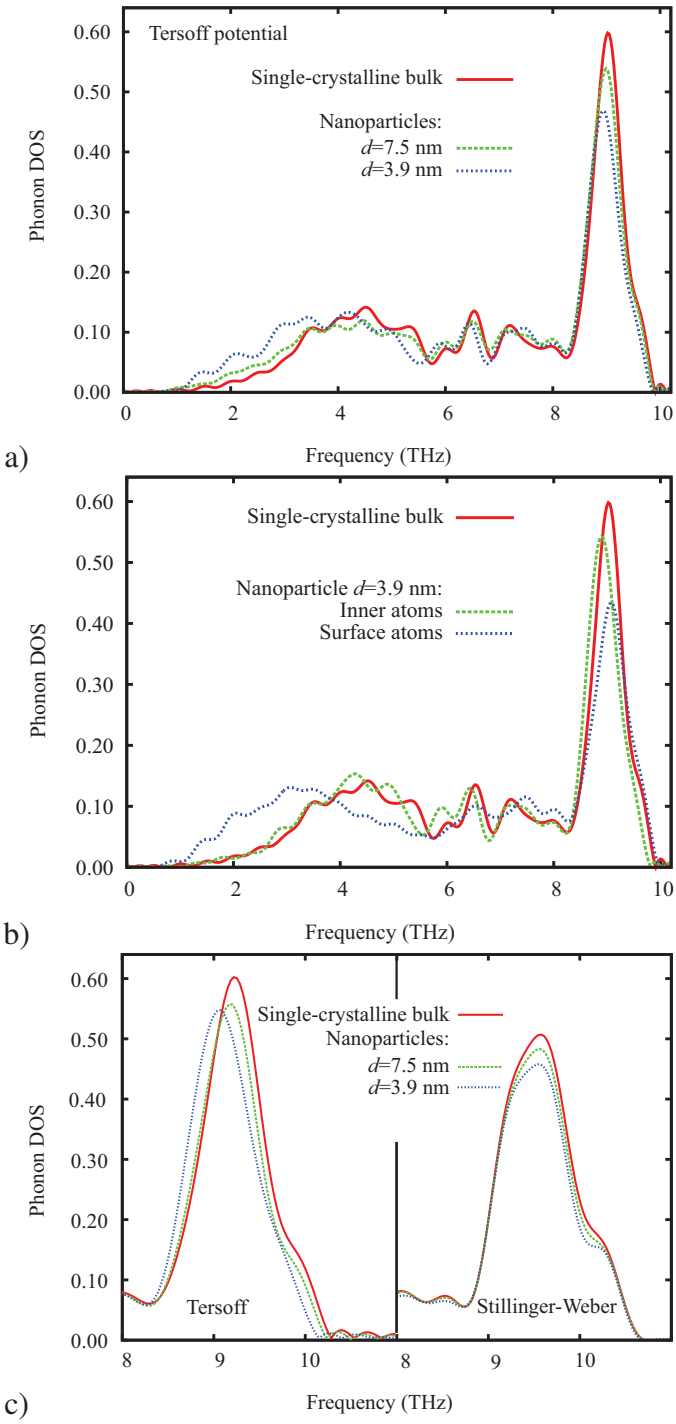

Figure 35: Phonon density of states for crystalline Ge-nanoparticles: a) PDOS of a single crystal compared with the PDOS of nanoparticles with a diameter of d=3.9 nm and d=7.5 nm. b) PDOS of a single crystal compared with the partial PDOS of the surface and center atoms of a nanoparticle with a diameter of d=3.9 nm. c) Partial PDOS for the center atoms in nanoparticles with diameter of d=3.9 nm and d=7.5 nm The left panel shows the calculation for the Tersoff-potential with surface stresses, while the right panel shows the same calculation using the Stillinger-Weber potential without surface stresses and therefore no frequency shift.

surface stress and therefore we only expect to see the result of phonon confinement effects. Indeed, the result (see Fig. 35c) shows no variation of the peak maximum of the optical modes. Only the shoulder at high frequencies is shifted and can therefore be attributed to a confinement effect due to the lack of vibrational modes close to the Γ point. This can be understood by considering the wave vector $|\mathbf{q}| \approx \pi/D$, where D is the particle diameter. Small values for q are only possible, if D is very large. If D is in the nanometer regime, however, the limiting case $q \to 0$ can not be reached. Therefore phonons with q close to zero are missing from the PDOS (see Fig. 43).

In return, the red-shift of the optical modes observed with the Tersoff potential can unambiguously be attributed to strain effects due to surface stresses. In case of Tersoff's Ge potential surface stresses are tensile, leading to a slight lattice expansion corresponding to an increase in interatomic bond length of about 0.1 %, which indicates a softening of interatomic force constant. All following calculations are conducted with the Tersoff potential only, since this potential provides a non-negligible and tensile surface stress in line with experimental data [112, 117, 49].

9.2.2 *Embedded Nanoparticles*

In a next step, we have studied the role of interface stresses by studying the case of a nanoparticle embedded in a glassy matrix. For this setup we expect to see an overlap of the contributions of the glassy matrix with the modes of the embedded particle, on which interface stresses are acting.

The bulk glass was prepared by rapid quenching of a melt (quench rate 5 K/ps) leading to an amorphous structure. In the resulting glass individual particles of different sizes were introduced. This time cubic shapes were chosen, in order to better control the thickness of crystal-glass interfaces. Prior to the PDOS calculations, each structure was again relaxed at 50 K in order to form physically reasonable interfaces between the glass and the particles.

In Fig. 36(a), the PDOS for three different cubic nanoparticles immersed in the glass are displayed and compared with the PDOS of the perfect crystal and the bulk glass. The total number of atoms for all three structures is about 64000. By decreasing the particle size, we find an increased PDOS in the low frequency and a decreased PDOS at the high frequency peak. The increase of the acoustic modes can be easily explained by the increase of the relative amount of the glassy phase with decreasing crystallite size. The PDOS of a glass displays a characteristic enhancement of the low frequency phonon modes due to the higher volume when compared with the crystalline phase.

Next, we checked if the vibrational modes of the glassy matrix extend into the inner part of the embedded nanoparticle. For this, the PDOS of an embedded nanoparticle and a free nanoparticle, both with the same geometry and diameter of d=7.8 nm, were calculated. First, we studied how the glassy matrix affects the PDOS of the

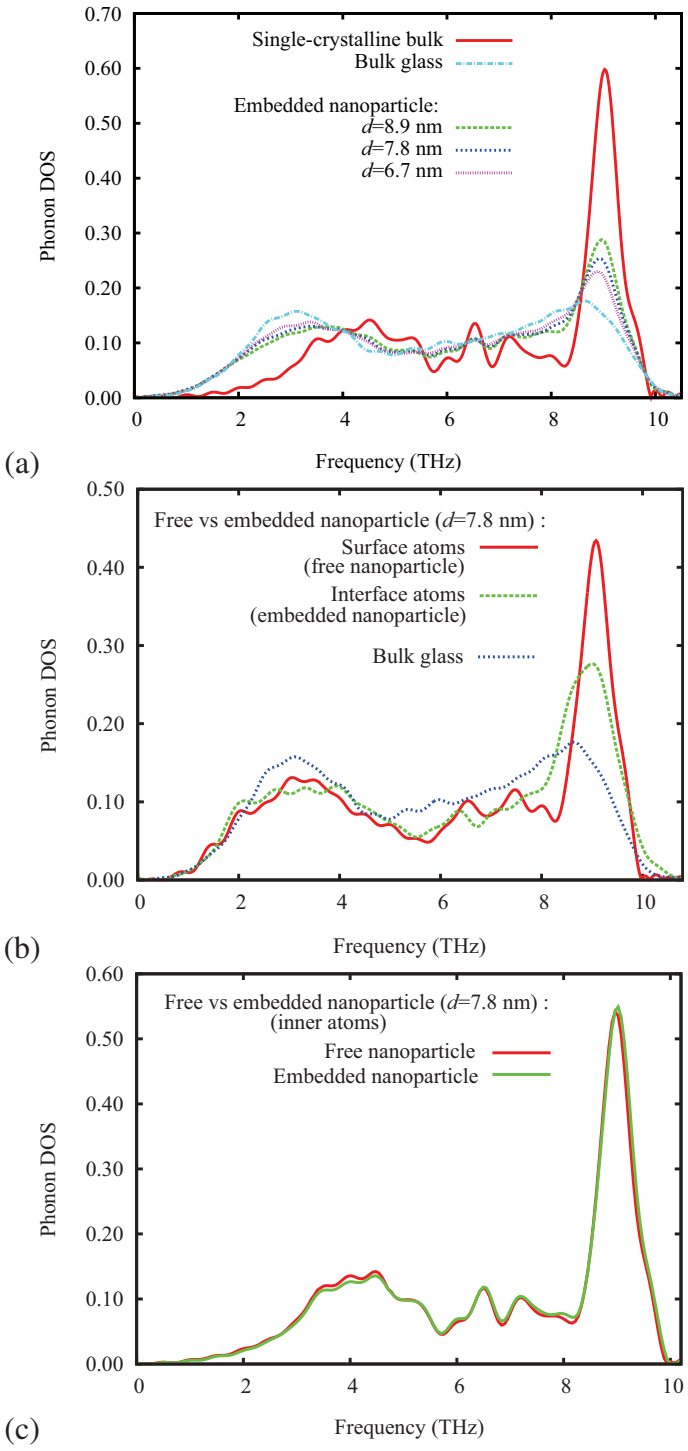

Figure 36: a) Total PDOS for three different nanoparticles with diameter of d=6.7 nm, d=7.8 nm and d=8.9 nm embedded in a glass, as compared to the perfect crystal and the bulk glass. b) Partial PDOS for interface and surface atoms of an embedded and free nanoparticle, respectively, in comparison to the bulk glass. c) Partial PDOS for inner atoms of a free and an embedded nanoparticle. In both cases the nanoparticle size is d=7.8 nm.

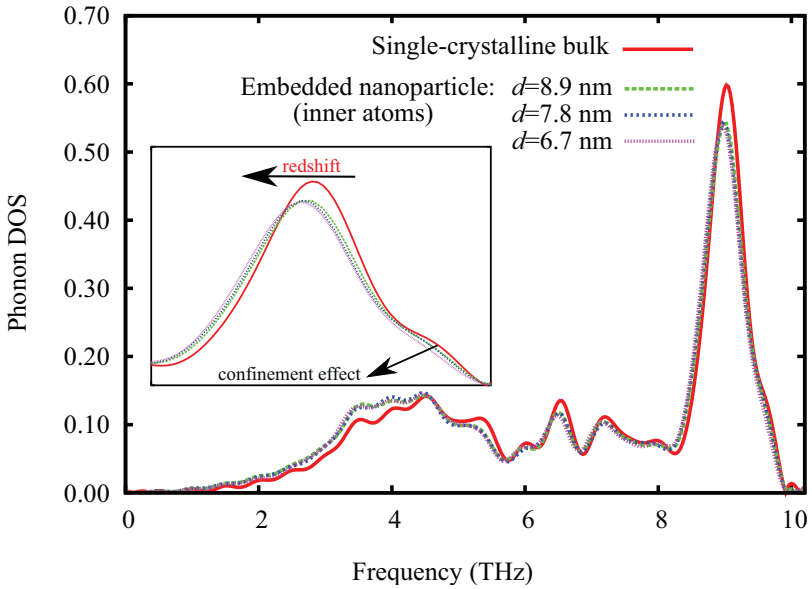

Figure 37: Partial PDOS for different nanoparticles embedded in the glass (only diamond atoms) as compared to the perfect crystal. The inset shows a magnification of the peak of the optical modes.

crystal-glass interface and compared to the PDOS of the surface and bulk glass. In Fig. 36(b), it can be seen that the partial PDOS of the interface atoms of the embedded nanoparticle differs strongly from the PDOS of the surface atoms of a free nanoparticle, and resembles more the PDOS of a bulk glass. This can be explained by the fact that glassy vibrational modes extend in the crystal-glass interfaces. Interface atoms are those which have nearest neighbor atoms in a diamond-like and glassy configuration, respectively. The calculated partial PDOS of the inner atoms of the embedded and free nanoparticle show no significant difference (Fig. 36(c)). Therefore, we can conclude that vibrational modes of the glassy matrix do not significantly affect the inner part of the embedded nanoparticle.

In fact, the nanoparticles which are embedded into the glassy structure show also the effect of homogeneous lattice expansion (shift of the PDOS towards lower frequencies). This can be seen from the partial PDOS of only inner atoms of the nanoparticles and as a function of size (Fig. 37). In analogy to the nanoparticle in vacuum, under free surface conditions, the nanoparticles in glass expand due to the interface stress which also in this case is tensile.

The disappearing shoulder on the main optical peak is again attributable to the confinement effect, which has been discussed in detail in the previous section (see inset in Fig. 37).

9.2.3 *Nanocrystalline structures*

The next setup studied was a nanocrystalline microstructure which can be understood as an ensemble of nanoparticles connected by "glassy-like" grain boundary areas. All structures were build by means of the Voronoi tesselation method [160]. Samples were prepared with 16 grains of 7.8 nm size, 54 grains of 5.2 nm size, 128 grains of 3.9 nm size and finally 5488 grains of 1.1 nm size. All nanocrystals were initially relaxed at 300 K for 100 ps and then cooled to 50 K prior PDOS calculations.

In Fig. 38(a) we present the PDOS as calculated for these nanocrystals and for the perfect crystal as well as the bulk glass. With decreasing particle size, the maximum of the low frequency region shifts slowly to lower frequencies and the peaks become broader. These features are connected to the ratio between the number of atoms in the grain boundaries and the number of atoms in the bulk-like regions. Due to the higher atomic disorder, the GBs show a signature similar to a glass. Additionally, GBs are characterized by an excess free volume preferentially leading to low frequency contributions to the PDOS.

In order to check the validity of our interpretation, we calculated the PDOS separately for atoms in GBs and in the grains. Fig. 38(a) shows the partial PDOS for grains with different sizes. As can be seen, the changes of PDOS for the grains in this nanocrystalline structure are essentially identical to the case of the nanoparticles immersed in the glass. Also in this case (inset of Fig. 39a), one can easily see the general shift towards lower frequencies with decreasing grain size. As mentioned in the previous section this behavior is indicative for a tensile interface stress. Previous simulation studies on Cu and Ni [46, 152] could not capture shifts in the PDOS with grain size. This is because fcc metals do not exhibit optical modes where finite-size effects due to surface stresses and confinement are most prominent. Moreover, the interatomic potentials used in these studies exhibit only a weak compressive surface stress, which has a minor influence on the sparsely populated acoustic modes. This is also the reason why a recent experimental study reported a close similarity of the PDOS of nanograins in nanocrystalline $Fe_{90}Zr_7B_3$ and α-Fe single crystals [47].

On the other hand, it can clearly be seen that the GBs are the strongest contributors to the increase in the acoustic modes of the PDOS (see Fig. 39b) due to a general broadening of the PDOS in those regions. Enhancement of the phonon modes both at low and high energy for GB atoms has been reported also earlier [47].

The increase of the acoustic low frequency modes in the PDOS will cause a direct change in the specific heat and the related thermal properties. In Fig. 5(b), together with the PDOS, we plot the excess specific heat for the three different nanocrystals as compared to the perfect crystal. With decreasing the grain size, or directly increasing the GB fraction, excess low frequency modes will be added, causing an increase in the excess specific heat.

Finally, it should be noted that grain sizes below 1.1 nm lead to unstable grains and result in an amorphous structure. This is in a good agreement with the smallest

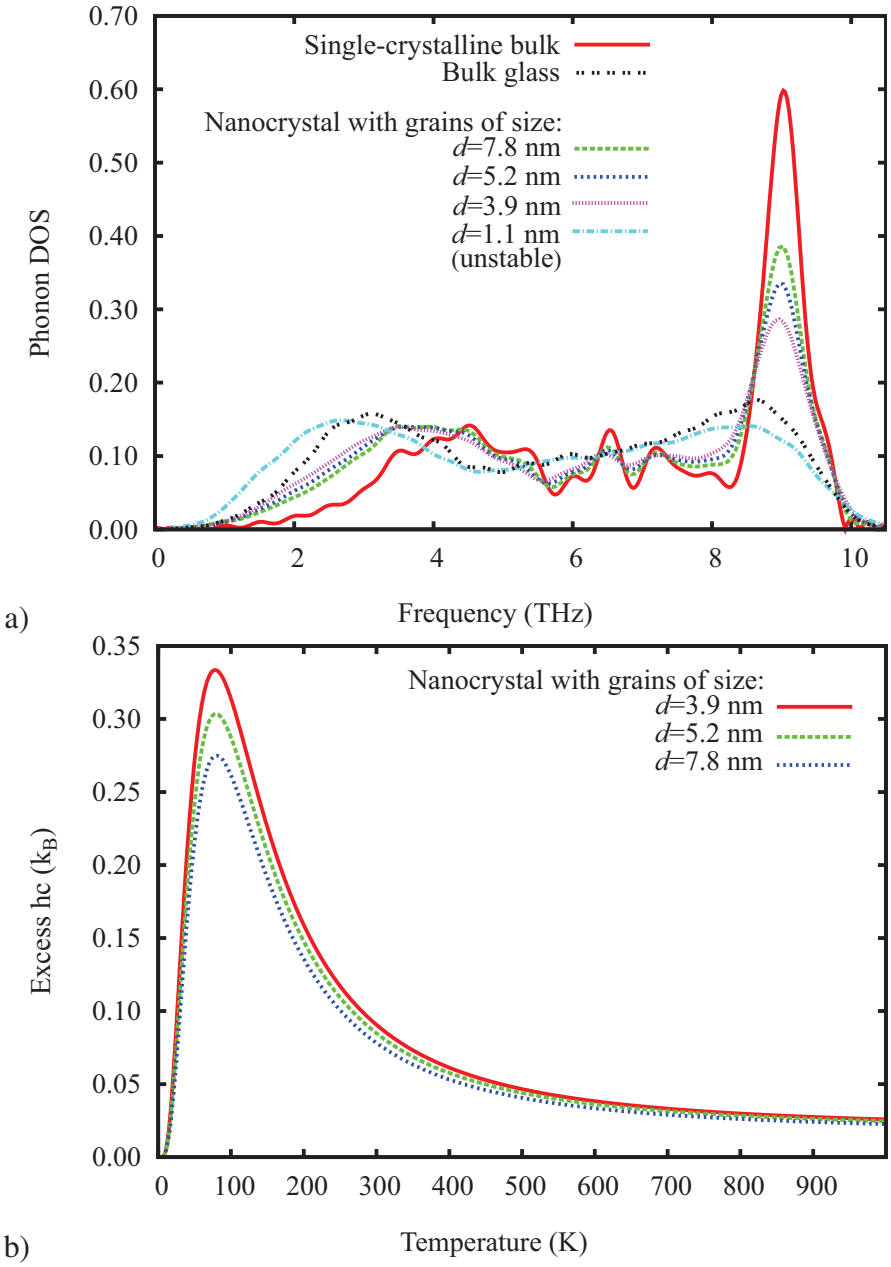

Figure 38: a) Total PDOS for nanocrystals with different grain sizes as compared to the perfect crystal and a bulk glass. b) Excess specific heat for three nanocrystals with grain sizes of d=3.9 nm, d=5.2 nm and d=7.8 nm as compared to a bulk crystal.

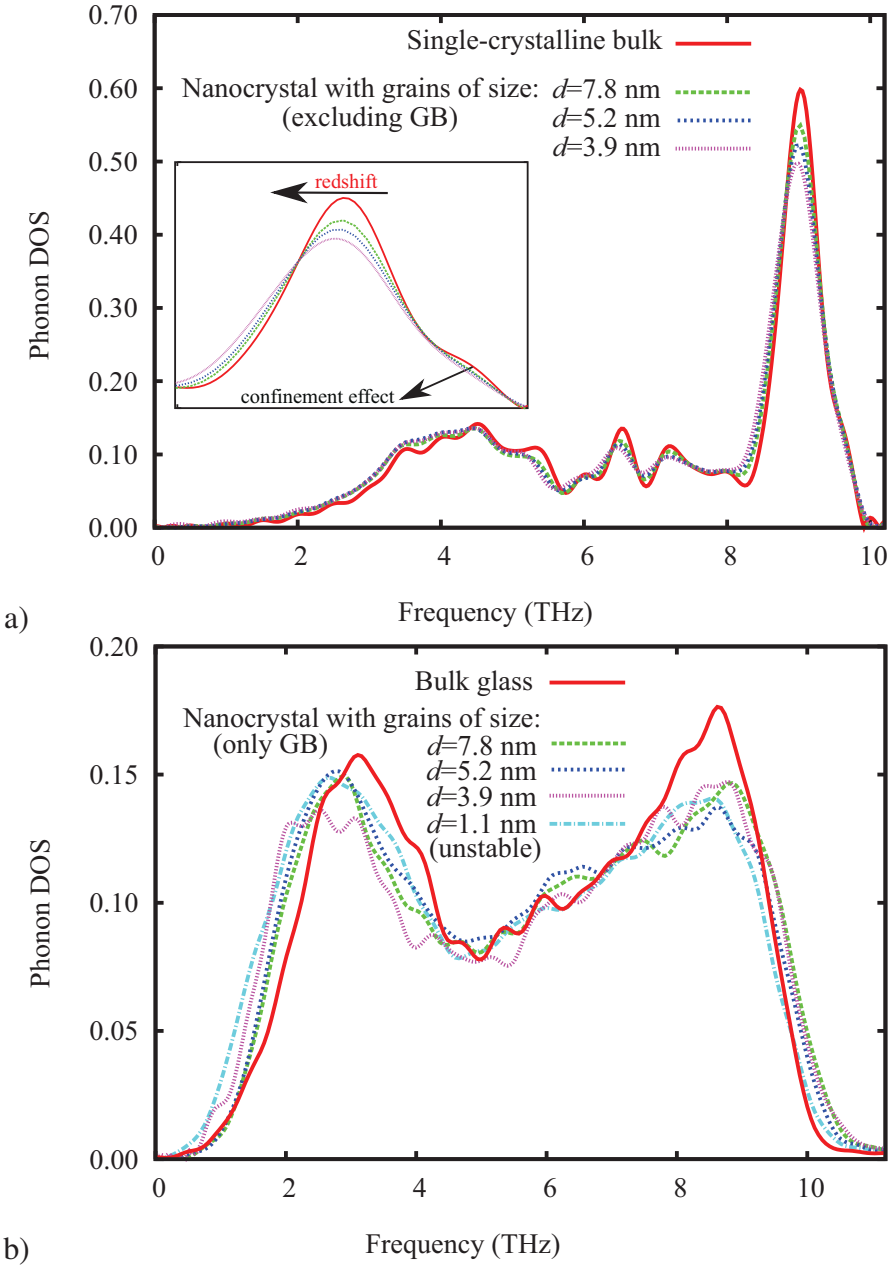

Figure 39: PDOS for three nanocrystals: a) for grains as compared to the perfect crystal (the inset shows a magnification of the peak of the optical modes), and b) for GB and resulting amorphous structure of NC with 1.1 nm grains as compared to the the bulk glass.

possible grain size for this material (1-2 nm) observed in experiments [161, 162]. The PDOS of this amorphous structure is different from the one calculated for a bulk glass; the acoustic branch is shifted to a lower frequency and is broader. This is due to a higher percentage of excess free volume in the amorphous state relative to the bulk glass. This new structure has an atomic volume of $V_{NC} \approx 24.86$ Å^3, whereas for the bulk glass the atomic volume is $V_{glass} \approx 23.03$ Å^3. The difference is about 8% and in good agreement with our previous results [163], where we have shown that it is possible to inject an excess free volume up to 8% at room temperature in a Ge glass.

9.2.4 *Ge nanoglass*

Next we return to the case of nanoglasses. First, we study the case of the Ge nanoglass. Because the consolidation process of a nanoglass involves the use of high pressure for powder compaction, also the atomic structure of the inner part of glassy droplets is affected, and in consequence its PDOS is changed as compared to the case of a bulk glass prepared by rapid quenching from the melt. Therefore in order to study the size effect on the PDOS as a function of the interface fraction and excess free volume localized in the interfaces, a simplified glass cubic model (64000 atoms) with a parallel set of glass-glass interfaces of identical thickness was studied (see Fig. 40a). The interfaces were randomly diluted by 10%, and relaxed at 300 K. The density distribution throughout the sample was monitored during the simulation. After relaxation, interfaces with 8% dilution were found. The calculated interface energy is 1.65 J/m^2.

We calculated the PDOS for two different nanoglass systems. The first one had one interface and the other one three interfaces with the same thickness (1 nm) and the same percentage of 8% free volume. In Fig. 40(a), we see how the acoustic peak shifts to a lower frequency with increasing number of interfaces. The excess free volume from the interfaces acts as a low frequency source for the phonon modes. In other words, an increase in excess free volume leads to an increase of low frequency modes in the PDOS. No shifting was observed in the optical modes, only a decrease in the optical peak amplitude due to the PDOS normalization (*i.e.* with respect to other peaks). This can be explained by a lower interface stress in a nanoglass compared to the interface stress calculated to a nanocrystalline structure. We found no considerable lattice expansion under interfaces stress, and, therefore, we expect no significant change in the PDOS of a nanoglass.

Fig. 8(b) shows the related excess specific heat with respect to the bulk glass. It exhibits a pronounced maximum at 80 K, which arises from the acoustic modes with lower frequencies [43] and grows with the number of interfaces. The optical modes provide only a minor contribution to the specific heat.

In order to check if phonon confinement depends on the interface thickness in nanoglasses, a similar procedure was followed for two cubic nanoglass structures with

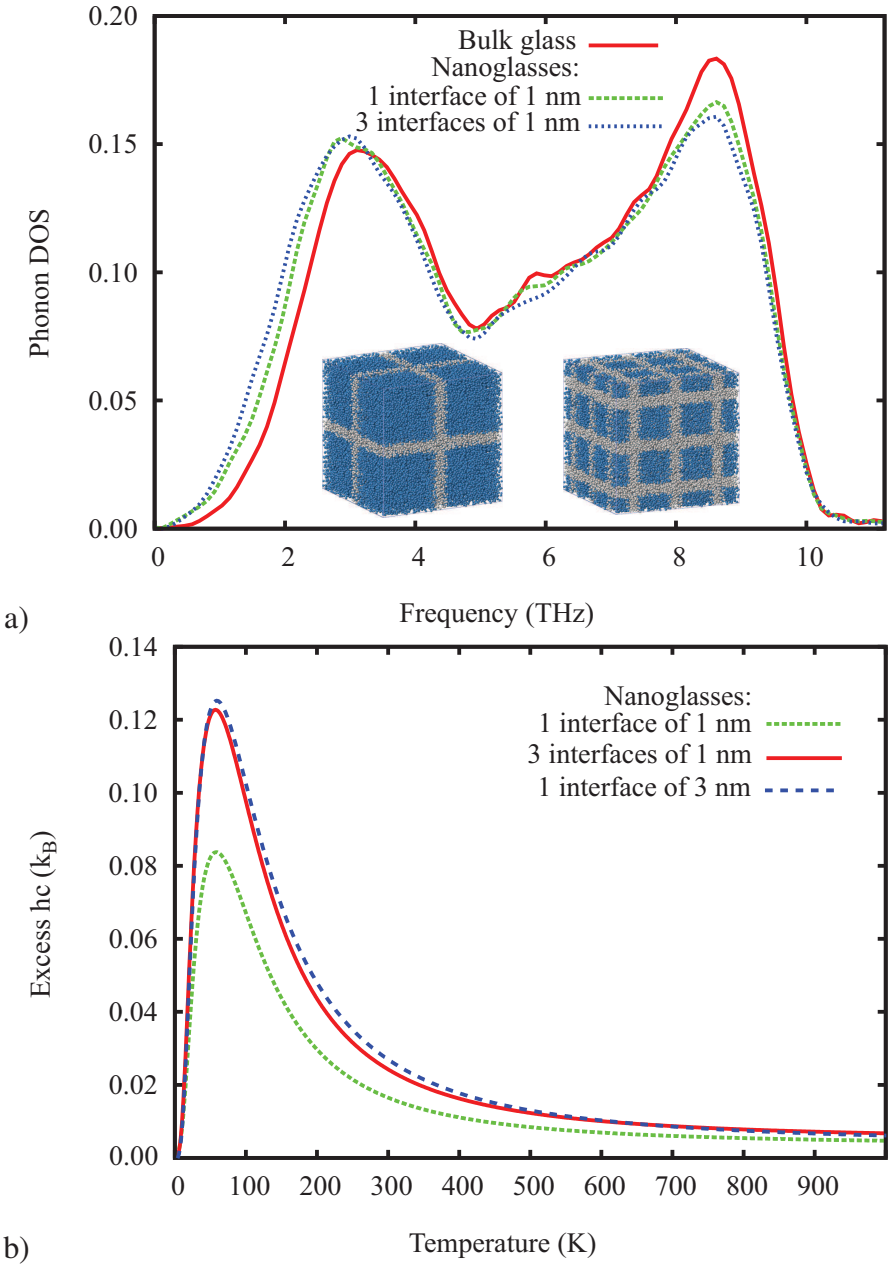

Figure 40: a) PDOS of a bulk glass compared with the PDOS of two nanoglasse: one with one interface of 1 nm and another with three interfaces of 1 nm. All interfaces have the same percentage of 8% free volume. b) Excess specific heat for these two nanoglasses and a third nanoglass with one interface of 3 nm as compared to the bulk glass.

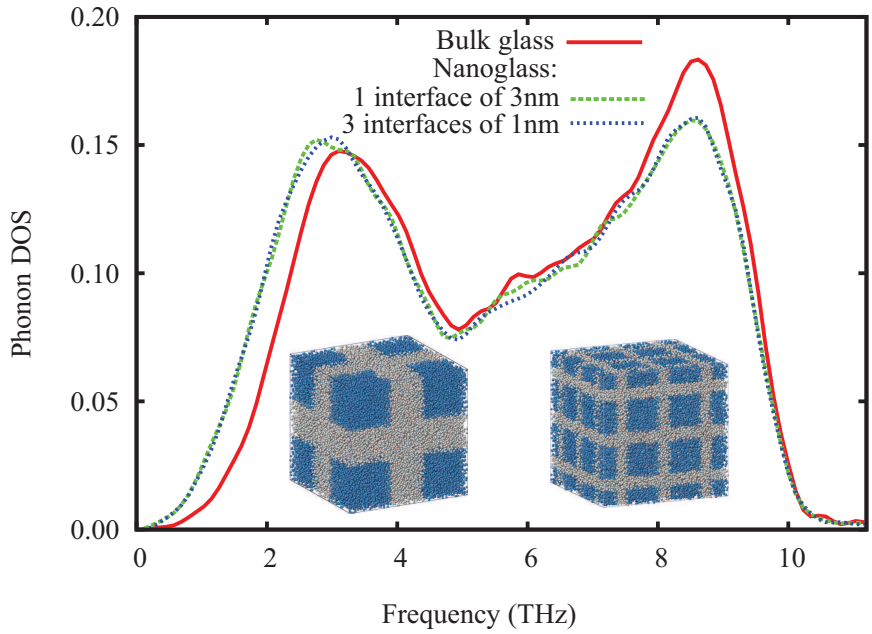

Figure 41: PDOS for bulk glass compared with the PDOS of two nanoglasses, first with one interface of 3 nm, and second with three interfaces of 1 nm. All interfaces have the same percentage of 8% free volume. The total amount of free volume is the same for both nanoglasses.

the same size; one with one interface of 3 nm, and another one with 3 interfaces of 1 nm, as can be seen in Fig. 41. The total excess free volume was approximately the same in both cases. It can be seen in Fig. 41, that no considerable difference in PDOS is observed for these cases. Furthermore, the excess specific heat of the two structures nearly superpose with extremely small differences (see Fig. 40(b)). This indicates that no extra phonon modes arise from the size effect. In summary, the origin of low frequency phonon modes is only due to the excess free volume in the interfaces.

9.2.5 $Cu_{64}Zr_{36}$ *nanoglass*

In the final part, we extend our investigations to the case of a metallic nanoglass, namely $Cu_{64}Zr_{36}$. Two type of nanoglasses (chemically homogeneous and inhomogeneous) were generated by compacting columnar grains with hexagonal cross section. The process of nanoglass compaction was presented in detail in Chapter 8. The pressure of 3 GPa used for powder compaction does not affect the atomic structure of the inner part of the glassy grains (for more informations see section 6.5.3). Consequently, for investigating the PDOS of $Cu_{64}Zr_{36}$ nanoglasses we resort no longer to the method used for studying the PDOS in case of the Ge nanoglass, by creating planar glass-glass interfaces in a cubic bulk glass by random dilution.

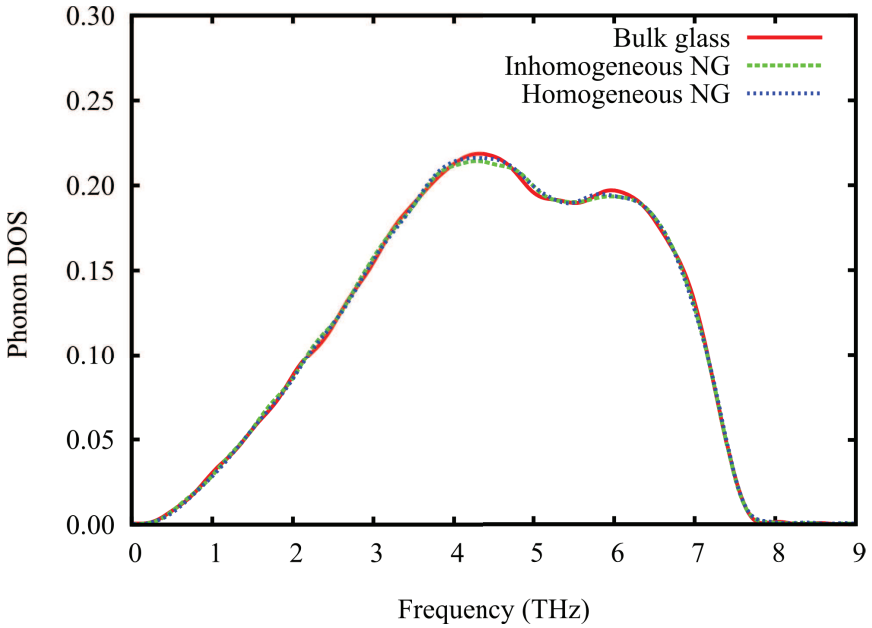

Figure 42: PDOS for bulk $Cu_{64}Zr_{36}$ glass compared with the PDOS of homogeneous (with homogeneous elements distribution) and inhomogeneous (with Cu-enriched interfaces) $Cu_{64}Zr_{36}$ nanoglasses.

As it was shown for case of the Ge nanoglass, the excess free volume (≈8%) localized in the interfaces modifies the PDOS by introducing vibrational modes at low frequencies. In the case of a $Cu_{64}Zr_{36}$ nanoglass, we found interfaces with a much lower fraction of excess free volume (≈ 1-2 %). Moreover, as a result of the initial setup the volume fraction of interfaces relative to the total volume of the nanoglass is much lower in comparison to the case of the Ge nanoglass. Based on our previous assumption that the PDOS of a nanoglass changes only due to the excess free volume, only weak differences between the PDOS of the $Cu_{64}Zr_{36}$ bulk glass and nanoglasses should be observable. As it can be seen in Fig. 42, the difference between the PDOS of the nanoglasses and the bulk glass are marginal. In other words, the $Cu_{64}Zr_{36}$ nanoglass contains a very low fraction of excess free volume and, therefore, the PDOS is not strongly affected. Interestingly, in the case of an inhomogeneous nanoglass, the presence of Cu-enriched interfaces does not change the PDOS significantly when compared to the PDOS of the bulk glass. In summary, only in a nanoglass with sufficient excess free volume new phonon modes with low frequency are added to the PDOS.

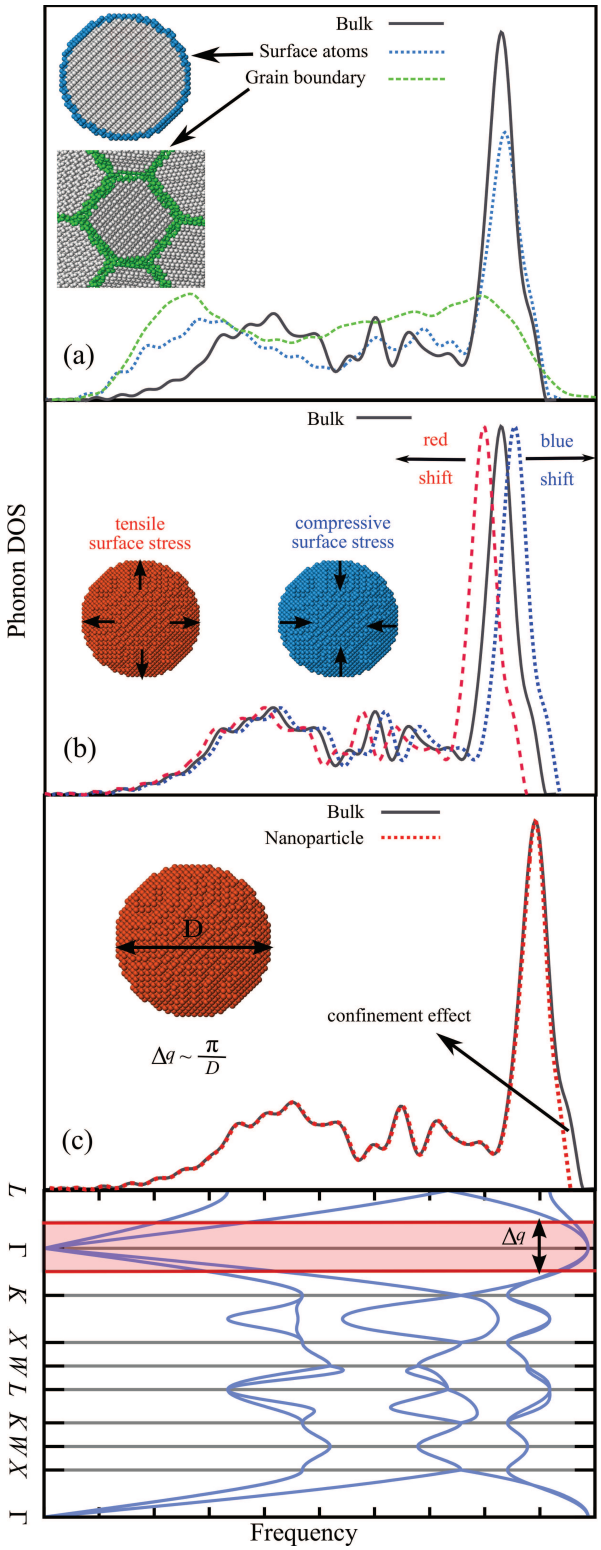

Figure 43: Size effects on PDOS: a) Nanostructural inhomogeneities, b) surface stresses, c) phonon confinement due to the finite particle size.

9.3 SUMMARY

In this study, we have investigated the lattice vibrations of different nanostructures for Ge as a prototype of a covalently bonded material. We identified which nanostructural discontinuities affect the phonon modes, realized a complete description of size effects on PDOS, and displayed the specific heat anomaly. We find three size effects (see Fig. 43) which change the PDOS as follow:

1. Nanostructural discontinuities (surface atoms, GBs, interfaces) characterized by a lower density in comparison with the bulk crystal cause an enhanced population of acoustical modes with low frequency, and a general broadening of PDOS due to the higher structural disorder.

2. Tensile (compressive) surface stresses result in a shift of the entire PDOS to lower (higher) frequencies.

3. Confinement due to the finite particle size caused the disappearance of several optical modes at the Brillouin zone center ($q = 0$).

We have systematically studied how these three size effects influence the PDOS of different nanostructured materials (nanoparticles, nanocrystals, embedded nanoparticles and nanoglasses). We have also shown that, all discontinuities (*e.g.* GBs, interfaces, surfaces) in nanostructures will introduce vibrational modes with low frequencies that directly affect the thermal properties of the material. In addition, we found that in the case of $Cu_{64}Zr_{36}$ nanoglasses the fraction of excess free volume is too small to influence their PDOS.

Part IV

SINGLE-COMPONENT METALLIC GLASS

10

THICKNESS DEPENDENCE OF GLASS TRANSITION

10.1 INTRODUCTION

For the stabilization of an amorphous structure in metallic materials at room temperature by quenching of a melt, generally more than two elements with different chemical properties are necessary. Multi-component alloys increase the complexity and size of the crystal unit cell and, therefore, decrease the crystal nucleation rate when quenching the liquid. However, by means of quenching except for Ge [26] no single-component metallic glass could be obtained so far. Moreover, Ge metallic glass has been obtained under special condition of high pressure.

Recently, Ghafari et al. reported the formation of the single-component Fe metallic glass in thin films deposited on an amorphous boron-doped cobalt-iron (a-CoFeB) [164]. They showed that multilayers of iron with a bcc structure and various thicknesses of 1 to 10 monolayers (ML) deposited on a-CoFeB substrate keep the crystalline structure up to a thickness of 6 layers. Decreasing the thickness of the Fe layer below 6 ML, an crystalline to amorphous transition in the iron layers occurred. The structure of the iron layer grown on top of an a-CoFeB layer is controlled by the energy between the Fe and a-CoFeB interface. Moreover, the non-collinear magnetic structure of amorphous Fe in combination with the soft magnetic properties of amorphous CoFeB lead to a magnetic behavior which is of interest for data recording devices. Transmission electron microscopy, X-ray diffraction studies as well as Mössbauer spectroscopy have been applied to prove the existence of single-component Fe glass, confined in the a-CoFeB substrate [164]. The iron-partial phonon density of states (PDOS) was measured showing dramatic differences between the amorphous and crystalline films. Experimental data shows that the formation of an amorphous iron layer is favorable for iron layers with thickness less than 6 ML.

In this section we study the crystalline to amorphous transition with film thickness for a single-component metallic glass, and extend the study of size effects in the phonon density of states (PDOS) to the case of metallic thin films.

10.2 RESULTS AND DISCUSSIONS

For a better understanding of the crystalline to amorphous transition phenomena and to prove the formation of a Fe single-component metallic glass, classic molecular dynamics (MD) simulations are carried out using the MD code LAMMPS. A Finnis-Sinclair many-body interaction potential, originally developed for the FeAl system was used in order to represent the interaction between the atoms [100]. We used this potential because there is no established potential for FeCo. However, the interatomic potential for AlFe provides a qualitatively reasonable description of the crystal to amorphous transition in thin films.

In order to simulate the deposition of crystalline atomic layers on an amorphous alloy, initially, an amorphous sample was prepared by melting a crystalline FeAl alloy consisting of 240000 atoms to 3000 K. By fast quenching from 3000 to 50 K, using a cooling rate of 0.1 K/ps an amorphous alloy was obtained. The amorphous structure was confirmed by common neighbor analysis, pair distribution function and PDOS. On top of this, two layers of crystalline Fe with (110) orientation and 12000 atoms were deposited. In the second attempt, six Fe layers with 36000 atoms and (110) orientation were deposited on top of the amorphous alloy. Periodic boundary conditions were applied in all directions, so that the crystalline part remains embedded in the amorphous matrix. After relaxation of all atoms for 50 ps at 50 K, the Fe atoms with two crystalline layers had become amorphous, as is shown in the insert on Fig.44(a). Increasing the number of Fe layers to six and repeating the same procedure, the iron layers remain crystalline after relaxation. These results are in good agreement with the experimental observations [164].

In addition, the PDOS of amorphous and crystalline Fe multilayers described above was computed from the Fourier transformation of the velocity autocorrelation function (VAC) [106] described in detail in section 4.4.1. Calculated and experimental PDOS have been always normalized for an easier comparison. The experimental PDOS curves corresponding to (amorphous) 2ML Fe and (crystalline) 6ML Fe are presented in Fig. 44(a). The calculated curves agree quite well with the experimental data (Fig. 44b).

Further, we extend the study of the size effects in the PDOS on the case of Fe thin layers. Fig. 44(a), shows two interesting features. First, the PDOS of the 6 crystalline Fe layers embedded in the AlFe glass exhibits no shift due to the interfaces stresses (explained in detail in chapter 9) when compared to the PDOS of the single-crystalline Fe bulk. Secondly, the PDOS of embedded crystalline multilayers is characterized by an increase of the high frequency modes between 40-50 meV. In case of a perfect crystal these modes are missing.

For explaining these features in the PDOS of the embedded multilayers we calculate PDOS of the same 6 multilayers with free surfaces in the direction in which the film was deposited on the glassy matrix. Also the PDOS of AlFe bulk glass is calculated. One can see in case of PDOS of the same 6 multilayers with free surfaces a general

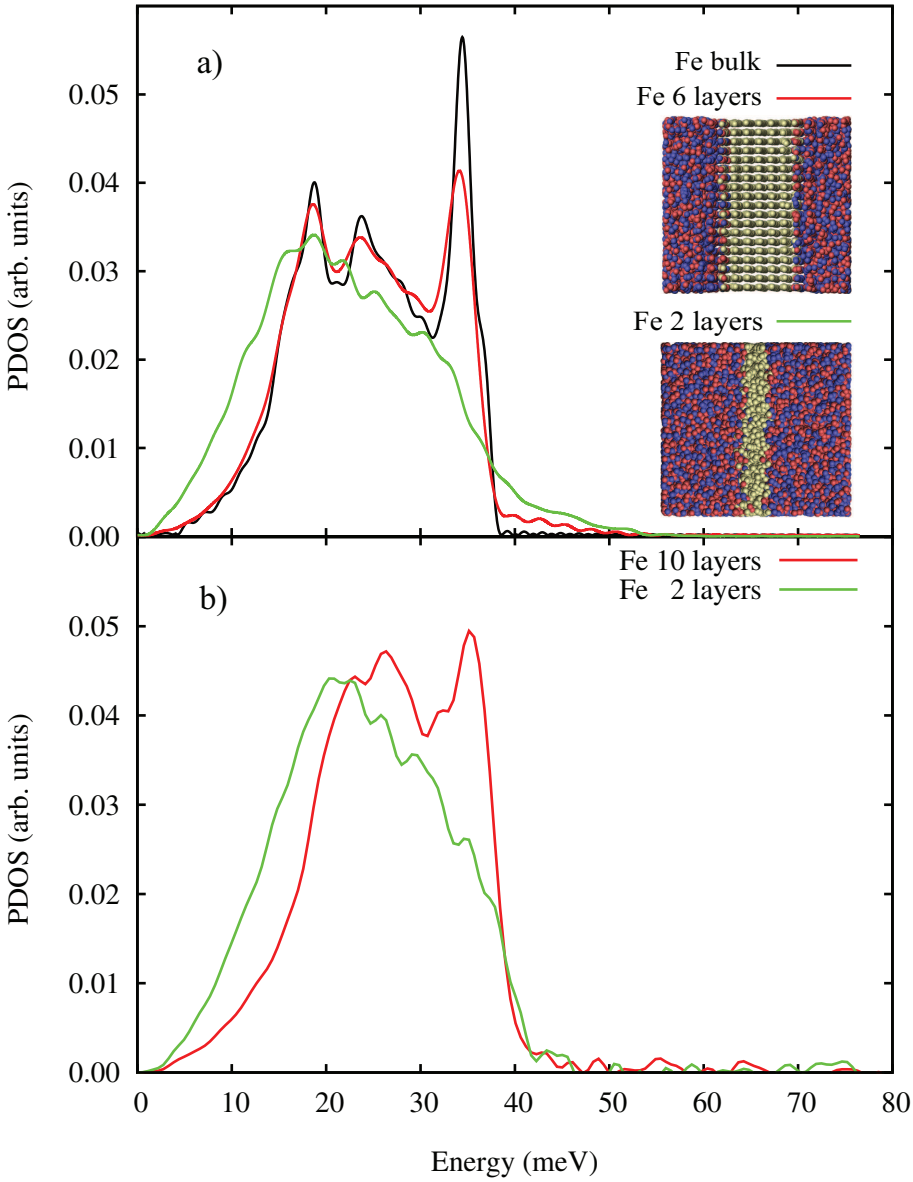

Figure 44: (a) Simulated iron partial DOS for 2 and 6 iron layers embedded between amorphous alloys (see text). The simulated structure (shown as insert) is for 2 iron layers amorphous and for 6 Fe layers crystalline. (b) The iron partial DOS of an a-CoFeB/Fe multilayer with 2 and ten Fe.

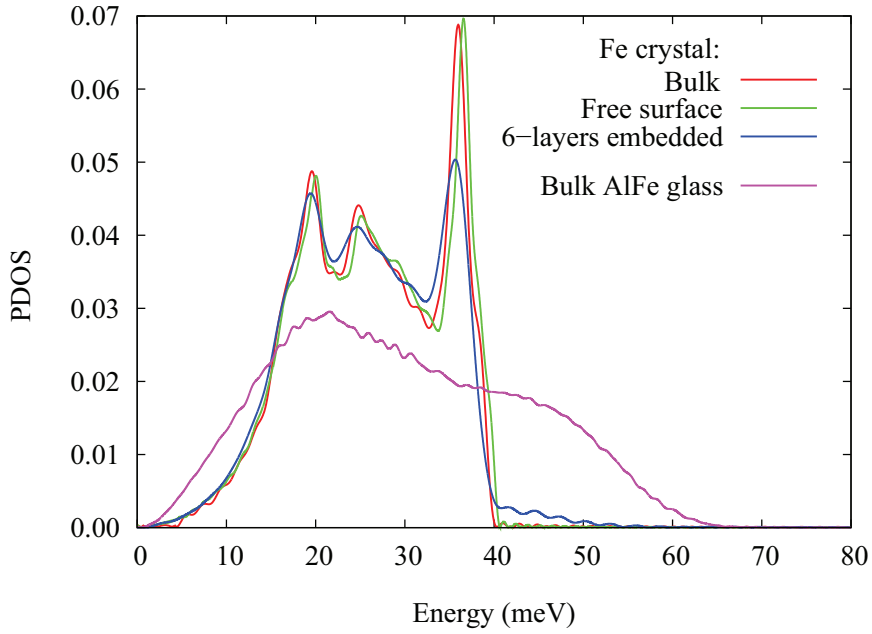

Figure 45: (a) Calculated PDOS for 6 crystalline Fe layers embedded between AlFe amorphous alloys and for the same 6-multilayers in vacuum in comparison to the PDOS of Fe perfect crystal and AlFe bulk glass.

shift to a higher frequency (blue shift), and the missing of the high frequency modes ranging between 40-50 meV (see Fig. 45). The blue shift, was explained in Chapter 9 by the compressive surface stress. Moreover, the blue shift is absent in the case of PDOS of embedded crystalline multilayers. This can be explained by a negligible interface stress in comparison to the surface stress. In Chapter 9 we found that glassy vibrational modes did not strongly affect the PDOS of Ge embedded nanoparticles, and stop at the crystal-glass interface. Moreover, in the case of Fe embedded crystalline multilayers, AlFe glassy vibrational modes extend over the whole sample affecting also the PDOS of the inner part of the embedded crystalline multilayers. This can be clearly seen in Fig. 45, where an increase in the population of the high frequency modes is induced in the PDOS of the Fe crystalline multilayers by the surrounding AlFe glassy matrix.

10.3 SUMMARY

We have studied the crystalline to amorphous transition of thin iron films in Fe/AlFe multilayers with decreasing Fe film thickness. The results provide evidence for the existence of single-component metallic glasses. In good agreement with experimental results, we found that the iron film maintains the crystalline structure for films thickness of 6 monolayers. Decreasing the thickness of the iron film to two monolay-

ers, the crystalline to amorphous transition takes place. Also, we used calculations of the PDOS to prove the crystalline to amorphous transition. The MD simulated PDOS agree quite reasonable with experimental data, reinforcing the aforementioned statements. Finally, we extend the study of size effects in the PDOS to the case of Fe embedded thin films. We found that interfaces stresses do not affect strongly the PDOS. Moreover, the vibrational modes of AlFe glass extend in the crystalline phase of embedded thin film adding extra vibrational modes to the PDOS.

CONCLUSIONS

In the present thesis, structural and mechanical and vibrational properties of nanoglasses were investigated by means of molecular dynamics simulations. In analogy to a nanocrystalline structure, a nanoglass can be obtained by compacting glassy nanoparticles. Indirect experimental results predicted that the resulting structure is characterized by glassy grains separated by interfaces. The largest part of this dissertation dealt with the characterization of interfaces and provided the atomic-level structure of inhomogeneities or interfaces in a nanoglass. A simple geometry of one planar glass-glass interface was constructed by contacting two relaxed glass surfaces. The structural analysis of a planar glass-glass interface is summarized in the following:

- An interface is characterized by a modified local topology (defective short range order) and higher fraction of excess free volume in comparison to the bulk glass. The maximum content of excess free volume localized within the interface is proportional to the glass yield strain.
- When the glass is annealed to an elevated temperature below the transition temperature, Cu-atoms segregate to the glass surface. Compacting these two surfaces, a glass-glass interface with an increased Cu-concentration and modified local topology formed.
- Both kinds of interfaces are stable at elevated temperature on MD time scales.
- Interfaces do not delocalize when compressed by a stress below the critical stress for shear band formation.

With these results, it is possible to prove Gleiter's predictions of a NG structure, providing direct evidence for the existence of interfaces.

Based on the results presented above, two kinds of nanoglass were constructed, a covalent Ge and a metallic CuZr nanoglass. Because the yield strain of the CuZr metallic glass is around 2%, also the excess free volume fraction in the interfaces was expected to be below this percentage. In case of a Ge nanoglass, due to a higher yield strain, interfaces can easily be visualized and are characterized by an excess free volume of about 8% at room temperature. Although metallic nanoglasses are characterized by interfaces with a small fraction of excess free volume, the local topology changes considerably when compared to the bulk values. Moreover, within these interfaces not only the topology but also the composition can be different

from the bulk glass. When consolidating a metallic glassy nanopowder, which was subjected to a pre-annealing process, a nanoglass with Cu-enriched interfaces formed.

The second section of this study characterized the mechanical properties of nanoglasses. First, we studied how the presence of soft inhomogeneities or interfaces affects the plastic deformation of nanoglasses. For this, two types of nanoglasses were constructed: homogeneous (with a homogeneous element distribution) and inhomogeneous (with Cu-enriched interfaces) nanoglasses, both free of pores. Under tensile deformation, both nanoglasses exhibit a homogeneous plastic deformation in a highly organized pattern of multiple shear bands, distributed through the whole sample, in contrast to a BMG, where the plastic deformation is confined in one dominant shear band. The shear banding is preferentially initiated in the interfaces or soft regions and these shear bands can distribute the applied strain more homogeneously. It can be anticipated that nanoglasses exhibit an enhanced ductility as compared to the BMG. Secondly, we found that by increasing the glassy nanoparticles size, i.e. by decreasing interface density the plastic deformation become more localized. Finally, we showed that in case of nanoglasses with pores, these discontinuities do not considerably affect the plastic deformation mechanism. Moreover, the deformation mechanism of a nanoglass can be easely tuned by thermal treatement or prior deformation. Therefore, similar to microstructural inhomogeneities in pre-deformed BMGs, the presence of interfaces in a nanoglass was found to improve the plastic behavior when compared to a BMG.

The next part of this dissertation presented a systematic study on the interplay of nanostructural features and lattice vibrations, where Germanium was used as a representative reference material. In the past, studies on the phonon density of states (PDOS) provided information on the microstructure of materials, and, therefore, studing the PDOS in nanoglasses could prove the interface existence. Because the role of various finite-size effects in the PDOS were not clear, first a study on how the microstructural discontinuities affect phonon modes was conducted and a complete description of size effects on the PDOS of each nanostructured material (nanoparticles, nanocrystals, embedded nanoparticles and nanoglasses) was realized. Three size effects which change the PDOS were indentified:

- Nanostructural discontinuities (surface atoms, GBs, interfaces), characterized by a lower density in comparison with the bulk crystal, cause an enhanced population of acoustical modes with low frequency and a general broadening of the PDOS due to the higher structural disorder.

- Tensile (compresive) surface stresses result in a shift of the entire PDOS to lower (higher) frequencies.

- Confinement due to the finite particle size caused the disappearance of several optical modes at the Brillouin zone center ($q = 0$).

For each of the nanostructures mentioned before, it was analyzed how the PDOS is influenced by the previous three effects. In case of crystalline nanostructured materials all three size effects have been identified while in case of amourphous nanoglass the PDOS changes only due to the excess free volume in the interfaces.

In the last part, a short chapter about the formation of a single-component metallic glass is presented. We found in accordance with experimental results that in case of Fe multilayers with bcc structure and thickness of 6 layers, deposited on amorphous AlFe, the film keeps the crystalline structure. Decreasing the thickness of the Fe film to 2 layers, a crystal-to-amorphous transition in the Fe layers occurred. The transition was also proven by calculating the PDOS showing a dramatic difference between the amorphous and crystalline film. In addition, we extended the study of size effects in the PDOS in the case of Fe embedded thin films in AlFe metallic glass. We found that the vibrational modes of AlFe glassy matrix extend in the crystalline Fe thin film.

In summary, the present thesis provided for the first time direct theoretical evidence for the existence of metallic nanoglasses. Moreover, this study contributes to the understanding of the atomic-scale structure and mechanical and vibrational properties, and paves the way towards the development of new bulk metallic glasses.

OUTLOOK

Nanoglasses, like conventional bulk metallic glasses are metastable structures and the glass properties are expected to change due to structural relaxation via thermally activated processes. Consequently, a study on diffusion processes in nanoglasses can provide useful information on long time stability and delocalization of interfaces. The delocalization of interface is assumed to be an alternative approach to form glasses with new atomic structure [165]. The excess free volume initially localized in the interface delocalizes over the entire nanoglass volume resulting in a new structure characterized by a different short-range order and density.

Concerning the study on mechanical properties of nanoglasses there are still many other aspects which deserve further investigation. In the present thesis, for studying mechanical properties of nanoglasses we used the $Cu_{64}Zr_{36}$ alloy because this composition has a high packing density [143, 88] and, therefore, high shear resistance. We found that the presence of interfaces or soft regions separating the hard glassy grains improves the nanoglass plasticity by promoting multiple shear bands. The next interesting question is to study if nanoglasses containing glassy grains with an alloy composition with low packing density or a soft phase combined with the $Cu_{64}Zr_{36}$ hard glassy grains would also exhibit a homogeneous plastic deformation similar to the case of chemically homogeneous nanoglasses. We showed that the thermal annealing process leads to a more localized plastic deformation in chemically homogeneous nanoglasses. In contrast, nanoglasses containing glassy grains with different alloy composition could keep the enhanced ductility even after thermal annealing.

It is also interesting to consider the case of multi-component nanoglasses. By compacting soft and hard glassy grains of different chemical elements the resulting nanoglass would possess the hardness of the hard glassy alloy and an improved plasticity provided by the soft alloy. Similar to nanoglasses with different alloy composition, multi-component nanoglasses could exhibit an homogeneous plastic deformation even after annealing.

With respect to the phonon density of states it would be interesting to extend our study to the thermodynamic properties of nanoglasses. Other thermodynamic quantities such as entropy, vibrational free energy, vibrational mean square amplitudes, and Debye temperatures can be calculated by means of the phonon density of states [166].

As described in Chapter 10, the formation of a single-element metallic glass in thin films is a function of the film thickness. More studies could provide quantitative results for the thickness dependence of the crystal-glass transition in thin films. It is still not fully understood if the interface energy is the main reason for the crystal-glass transition. Further, it would be fruitful to study the crystalline-glass nanolaminates

under deformation. It was shown that nanolamitates show increased ductility due to the presence of a crystalline phase [167]. By decreasing the crystalline layer thickness the properties of nanolamitates vary. We showed that the crystalline layers thickness can be decreased up to a critical thickness where the crystalline layers amorphise. Deformation could decrease the stability of the crystalline layers and even for layers wider than the critical thickness, the crystal-glass transition could occurs under deformation. As a result, we expect the formation of glass-glass nanolaminates.

ERKLÄRUNG – DISCLAIMER

Die vorliegende Arbeit wurde im Zeitraum von Mai 2007 bis August 2010 im Fachgebiet Materialmodellierung am Institut für Materialwissenschaft der Technischen Universität Darmstadt bei Herrn Prof. Dr. rer. nat. Karsten Albe angefertigt.

Hiermit versichere ich an Eides statt, dass ich die vorliegende Arbeit selbstständig und nur unter Verwendung der angegebenen Hilfsmittel angefertigt habe. Von mir wurde weder an der Technischen Universität Darmstadt noch an einer anderen Hochschule ein Promotionsversuch unternommen.

Darmstadt, den 5. Juli 2011

Daniel Şopu

ACKNOWLEDGMENTS

At this point I would like to thank a number of people without whom I could not have accomplished this work and finished my thesis. First, I want to thank my advisor Professor Karsten Albe for his continued support and the confidence placed in me. I appreciate all his contributions of time, ideas, and funding to make my Ph.D. experience productive.

Professor Horst Hahn, I would like to thank you for evaluating my work.

I am very grateful to Professor Herbert Gleiter, for the idea of my project and for useful discussions.

Thank very much my colleagues from the Department of Materials Modeling for the pleasant time we have spent together. This also applies to Renate Hernichel who also offered me a great help in many organizational things. My office colleagues, Yvonne Ritter and Alexander Stukowski I am grateful for innumerable technical discussions and for the pleasant time. Yvonne Ritter deserves special thanks for the support with some of her results included in section 7. Also many thanks to Peter Agoston for fruitful discussions and giving encouragements in the difficult times over the last four years. My colleague Manuel Diehm has supported me in the final correction of the thesis. Many thanks to Jani Kotakoski for joint work which is presented in Chapter 9.

I wish to thank Kai Nordlund from the University of Helsinki, for teaching me the first basics of MD simulations through his online tutorials.

I also thank Professor Mihai Girtu, my first mentor, who advised me to do my PhD.

Nu in ultimul rand, doresc sa le multumesc parintilor mei care mi-au oferit tot suportul material si moral dea lungul studiilor mele. Totodata, vreau sa multumesc prietenei mele care m-a incurajat si a fost langa mine in momentele dificile.

This work was funded by the Deutsche Forschungsgemeinschaft by the research group DFG AL-578-5, 'Metallic nanoglasses'. Computing time was granted by the Research Centre Julich and the Center for Scientific Computing at Goethe University in Frankfurt.

CURRICULUM VITAE

Education

Master in Physics, July 2006

Ovidius University Constanta, Romania

Diploma in Mathematics and Physics, July 2005

Ovidius University Constanta, Romania

High School Graduation (Abitur), June 2001

Mihail Sebastian, Braila, Romania

Research experience

Research scientist, PhD student, since May 2007

Materials Modeling Division, Institute of Materials Science,

Technical University of Darmstadt, Germany

Research scientist (6 months), 2006

Faculty of Physics, Chemistry and Petroleum Technology

Ovidius University Constanta, Romania

Physicist (10 months), 2006

Rompetrol Quality Control,

Member company of Rompetrol Group, Constanta, Romania

Publications based on the present dissertation

1. D. Sopu, J. Kotakoski, and K. Albe, *Finite-size effects in the phonon density of states of nanostructured germanium: A comparative study of nanoparticles, nanocrystals, nanoglasses and bulk phases*, Phys. Rev. B 83, 245416 (2011)

2. D. Sopu, Y. Ritter, H. Gleiter, and K. Albe, *Deformation behavior of bulk and nanoscale metallic glasses studied via molecular dynamics simulations*, Phys. Rev. B 83, 100202 (2011)

3. D. Sopu, K. Albe, Y. Ritter, and H. Gleiter, *From nanoglasses to bulk massive glasses*, Appl. Phys. Lett. 94, (2009)

4. Y. Ritter, D. Sopu, and K. Albe. *Structure, stability and properties of internal interfaces in metallic glass*, Acta Mater. 59, 6588 (2011)

Other publications

1. D. Sopu, D.M. Popovici, and M.A. Girtu, *Molecular dynamics simulation of defect formation in irradiated Cu*, J. Optoelectr. Adv. Mater. 9, 799 (2007).

2. D. Sopu and M. A. Girtu, *Molecular dynamics simulations of the time evolution of irradiation induced defects*, Six International Conference of the Balkan Physical Union 899, (2007)

BIBLIOGRAPHY

[1] **Klement, W., Willens, R. H.** and **Duwez, P.**, *Noncrystalline structure in solidified gold-silicon alloys*, Nature, Vol. 187, No. 4740, pp. 869, 1960.

[2] **Jing, J., Kramer, A., Birringer, R., Gleiter, H.** and **Gonser, U.**, *Modified atomic structure in a Pd-Fe-Si nanoglass : A Mossbauer study*, J. Non-Cryst. Solids, Vol. 113, No. 2-3, pp. 167, 1989.

[3] **Weissmueller, J., Birringer, R.** and **Gleiter, H.**, *Nanostructured crystalline and amorphous solids*, Key Eng. Mater., Vol. 77-78, No. 77-78, pp. 161, 1993.

[4] **Weissmueller, J., Birringer, R.** and **H, G.**, *Microcomposites and nanophase materials*, Proc. of the TMS Annual Meeting New Orleans, p. 291, 1991.

[5] **Weissmueller, J., Schubert, P., Franz, H., Birringer, R.** and **Gleiter, H.**, *Nanostructured amorphous solids*, Proc. VII Natl. Conf. on the Physics of Non-Crystall. Solids Cambridge, England August 4-9, 1991.

[6] **Basu, J.** and **Ranganathan, S.**, *Bulk metallic glasses: A new class of engineering materials*, Sadhana, Vol. 28, pp. 783, 2003.

[7] **Greer, A. L.**, *Metallic glasses*, Science, Vol. 267, No. 5206, pp. 1947, 1995.

[8] **Eckert, J., Schultz, L., Hellstern, E.** and **Urban, K.**, *Glass-forming range in mechanically alloyed Ni-Zr and the influnece of the milling intensity*, J. Appl. Phys., Vol. 64, No. 6, pp. 3224, 1988.

[9] **Cahn, R. W. Greer, A. L.**, *Metastable states of alloys*, Phys. Metall., Vol. Elsevier Science., pp. 1724, 1996.

[10] **Chen, H.** and **Turnbull, D.**, *Formation, stability and structure of palladium-silicon based alloy glasses*, Acta Metall, Vol. 17, No. 8, pp. 1021, 1969.

[11] **Chen, H.**, *Thermodynamic considerations on the formation and stability of metallic glasses*, Acta Metall., Vol. 22, pp. 1505, 1974.

[12] **Liebermann, H.** and **Graham, C.**, *Production of amorphous alloy ribbons and effects of apparatus parameters on ribbon dimensions*, IEEE Trans. Magn., Vol. 12, pp. 921, 1976.

[13] **Drehman, A. J., Greer, A. L.** and **Turnbull, D.**, *Bulk formation of a metallic-glass Pd40Ni40P20*, Appl. Phys. Lett., Vol. 41, No. 8, pp. 716, 1982.

[14] **Kui, H. W., Greer, A. L.** and **Turnbull, D.**, *Formation of bulk metallic glass by fluxing*, Appl. Phys. Lett., Vol. 45, No. 6, pp. 615, 1984.

[15] **Inoue, A., Zhang, T.** and **Masumato, T.**, *Al-La-Ni amorphous-alloys with a wide supercooled liquid region*, Mater. Trans., JIM, Vol. 30, No. 12, pp. 965, 1989.

[16] **Inoue, A., Zhang, T.** and **Masumato, T.**, *Production of amorphous cylinder and sheet of $La_{55}Al_{25}Ni_{20}$ alloy by a metallic mold casting method*, Mater. Trans., JIM, Vol. 31, No. 5, pp. 425, 1990.

[17] **Oguchi, M., Inoue, A., Yamaguchi, H.** and **Masumato, T.**, *Production of Al-based amorphous sheets with large thickness by a supercooled liquid-quenching method*, J. Mater. Sci. Lett., Vol. 10, No. 5, pp. 289, 1991.

[18] **Peker, A.** and **Johnson, W. L.**, *A highly processable metallic glass - $Zr_{41.2}Ti_{13.8}Cu_{12.5}Ni_{10.0}Be_{22.5}$*, Appl. Phys. Lett., Vol. 63, No. 17, pp. 2342, 1993.

[19] **Telford, M.**, *The case for bulk metallic glass*, Mater. Today, Vol. 7, No. 3, pp. 36, 2004.

[20] **Pampillo, C. A.**, *Flow and fracture in amorphous alloys*, J. Mater. Sci., Vol. 10, No. 7, pp. 1194, 1975.

[21] **Gebert, A., Buchholz, K., Leonhard, A., Mummert, K., Eckert, J.** and **Schultz, L.**, *Investigations on the electrochemical behaviour of Zr-based bulk metallic glasses*, Mater. Sci. Eng., A, Vol. 267, No. 2, pp. 294–300, 1999.

[22] **Loffler, J. F.**, *Bulk metallic glasses*, Intermetallics, Vol. 11, No. 6, pp. 529, 2003.

[23] *Liquidmetal Technologies*
http://www.liquidmetal.com.

[24] **Wang, W. H., Dong, C.** and **Shek, C. H.**, *Bulk metallic glasses*, Mater. Sci. Eng. R-reports, Vol. 44, No. 2-3, pp. 45, 2004.

[25] **Wang, W. H., Lewandowski, J. J.** and **Greer, A. L.**, *Understanding the glass-forming ability of $Cu_{50}Zr_{50}$ alloys in terms of a metastable eutectic*, J. Mater. Res., Vol. 20, No. 9, pp. 2307, 2005.

[26] **Bhat, M. H., Molinero, V., Soignard, E., Solomon, V. C., Sastry, S., Yarger, J. L.** and **Angell, C. A.**, *Vitrification of a monatomic metallic liquid*, Nature, Vol. 448, No. 7155, pp. 787, 2007.

[27] **Gu, X. J., Poon, S. J.** and **Shiflet, G. J.**, *Mechanical properties of iron-based bulk metallic glasses*, J. Mater. Res., Vol. 22, No. 2, pp. 344, 2007.

[28] *Glassy Metals*
http://discovermagazine.com/2004/apr/glassy-metals.

[29] **Kawamura, Y., Kato, H., Inoue, A.** and **Masumoto, T.**, *Fabrication of bulk amorphous alloys by powder consolidation*, Int. J. Powder Metall, Vol. 33, No. 2, pp. 50, 1997.

[30] **Kato, H., Kawamura, Y., Inoue, A.** and **Masumoto, T.**, *Bulk glassy Zr-based alloys prepared by consolidation of glassy alloy powders in supercooled liquid region*, Mater. Sci. Eng., A, Vol. 226, pp. 458, 1997.

[31] **Gleiter, H.**, *Nanocrystalline solids*, J. Appl. Crystallogr., Vol. 24, No. 2, pp. 79, 1991.

[32] **Karaman, I., Robertson, J., Im, J. T., Mathaudhu, S. N., Luo, Z. P.** and **Hartwig, K. T.**, *The effect of temperature and extrusion speed on the consolidation of zirconium-based metallic glass powder using equal-channel angular extrusion*, Metall. Mater. Trans. A, Vol. 35A, No. 1, pp. 247, 2004.

[33] **Lee, M. H., Lee, K. S., Das, J., Thomas, J., Kuhn, U.** and **Eckert, J.**, *Improved plasticity of bulk metallic glasses upon cold rolling*, Scr. Mater., Vol. 62, No. 9, pp. 678, 2010.

[34] **Li, Q. K.** and **Li, M.**, *Atomic scale characterization of shear bands in an amorphous metal*, Appl. Phys. Lett., Vol. 88, No. 24, pp. 241903, 2006.

[35] **Cao, A. J., Cheng, Y. Q.** and **Ma, E.**, *Structural processes that initiate shear localization in metallic glass*, Acta Mater., Vol. 57, No. 17, pp. 5146, 2009.

[36] **Hofmann, D. C., Suh, J. Y., Wiest, A., Duan, G., Lind, M. L., Demetriou, M. D.** and **Johnson, W. L.**, *Designing metallic glass matrix composites with high toughness and tensile ductility*, Nature, Vol. 451, No. 7182, pp. 1085, 2008.

[37] **Scudino, S., Surreddi, K. B.** and **Eckert, J.**, *Mechanical properties of cold-rolled* $Zr_{60}Ti_5Ag_5Cu_{12.5}Ni_{10}Al_{7.5}$ *metallic glass*, Phys. Status Solidi A, Vol. 207, No. 5, pp. 1118, 2010.

[38] **Cao, Q. P., Liu, J. W., Yang, K. J., Xu, F., Yao, Z. Q., Minkow, A., Fecht, H. J., Ivanisenko, J., Chen, L. Y., Wang, X. D., Qu, S. X.** and **Jiang, J. Z.**, *Effect of pre-existing shear bands on the tensile mechanical properties of a bulk metallic glass*, Acta Mater., Vol. 58, No. 4, pp. 1276, 2010.

[39] **Hays, C. C., Kim, C. P.** and **Johnson, W. L.**, *Microstructure controlled shear band pattern formation and enhanced plasticity of bulk metallic glasses containing in situ formed ductile phase dendrite dispersions*, Phys. Rev. Lett., Vol. 84, No. 13, pp. 2901, 2000.

[40] **Hays, C. C., Kim, C. P.** and **Johnson, W. L.**, *Improved mechanical behavior of bulk metallic glasses containing in situ formed ductile phase dendrite dispersions*, Mater. Sci. Eng., A, Vol. 304, pp. 650, 2001.

[41] **He, G., Eckert, J., Loser, W.** and **Schultz, L.**, *Novel Ti-base nanostructure-dendrite composite with enhanced plasticity*, Nat. Mater., Vol. 2, No. 1, pp. 33, 2003.

[42] **Xie, S.** and **George, E. P.**, *Size-dependent plasticity and fracture of a metallic glass in compression*, Intermetallics, Vol. 16, No. 3, pp. 485, 2008.

[43] **Wolf, D., Wang, J., Phillpot, S. R.** and **Gleiter, H.**, *Phonon-induced anomalous specific heat of a nanocrystalline model material by computer simulation*, Phys. Rev. Lett., Vol. 74, No. 23, pp. 4686, 1995.

[44] **Yang, C. C.** and **Li, S.**, *Size-dependent raman red shifts of semiconductor nanocrystals*, J. Phys. Chem. B, Vol. 112, No. 45, pp. 14193, 2008.

[45] **Rodden, W. S. O., Torres, C. M. S.** and **Ironside, C. N.**, *Three-dimensional phonon confinement in CdSe microcrystallites in glass*, Semicond. Sci. Technol., Vol. 10, No. 6, pp. 807, 1995.

[46] **Derlet, P. M., Meyer, R., Lewis, L. J., Stuhr, U.** and **Van Swygenhoven, H.**, *Low-frequency vibrational properties of nanocrystalline materials*, Phys. Rev. Lett., Vol. 87, No. 20, pp. 205501–, 2001.

[47] **Stankov, S., Yue, Y. Z., Miglierini, M., Sepiol, B., Sergueev, I., Chumakov, A. I., Hu, L., Svec, P.** and **Ruffer, R.**, *Vibrational properties of nanograins and interfaces in nanocrystalline materials*, Phys. Rev. Lett., Vol. 100, No. 23, pp. 235503, 2008.

[48] **Kara, A.** and **Rahman, T. S.**, *Vibrational properties of metallic nanocrystals*, Phys. Rev. Lett., Vol. 81, No. 7, pp. 1453–, 1998.

[49] **Ahmad, M. I.** and **Bhattacharya, S. S.**, *Size effect on the lattice parameters of nanocrystalline anatase*, Appl. Phys. Lett., Vol. 95, No. 19, pp. 191906, 2009.

[50] **Krenzer, B., Hanisch-Blicharski, A., Schneider, P., Payer, T., Mollenbeck, S., Osmani, O., Kammler, M., Meyer, R.** and **von Hoegen, M. H.**, *Phonon*

confinement effects in ultrathin epitaxial bismuth films on silicon studied by time-resolved electron diffraction, Phys. Rev. B, Vol. 80, No. 2, pp. 024307, 2009.

[51] **Weissmuller, J., Birringer, R.** and **Gleiter, H.**, *Short-range disordered Si-Au alloy - Evidence for a new phase*, Phys. Lett. A, Vol. 145, No. 2-3, pp. 130, 1990.

[52] **Dyre, J. C.**, *Colloquium: The glass transition and elastic models of glass-forming liquids*, Rev. Mod. Phys., Vol. 78, No. 3, pp. 953, 2006.

[53] **Cohen, M. H.** and **Turnbull, D.**, *Molecular transport in liquids and glasses*, J. Chem. Phys., Vol. 31, No. 5, pp. 1164, 1959.

[54] **Turnbull, D.** and **Cohen, M. H.**, *Free-volume model of amorphous phase - Glass transition*, J. Chem. Phys., Vol. 34, No. 1, pp. 120, 1961.

[55] **Turnbull, D.** and **Cohen, M. H.**, *On free-volume model of liquid-glass transition*, J. Chem. Phys., Vol. 52, No. 6, pp. 3038, 1970.

[56] **Cohen, M. H.** and **Grest, G. S.**, *Liquid-glass transition, a free volume approach*, Phys. Rev. B, Vol. 20, No. 3, pp. 1077, 1979.

[57] **Miracle, D. B.**, *The efficient cluster packing model - An atomic structural model for metallic glasses*, Acta Mater., Vol. 54, No. 16, pp. 4317, 2006.

[58] **Li, M., Wang, C. Z., Hao, S. G., Kramer, M. J.** and **Ho, K. M.**, *Structural heterogeneity and medium-range order in Zr_xCu_{100-x} metallic glasses*, Phys. Rev. B, Vol. 80, No. 18, pp. 184201, 2009.

[59] **Cheng, Y. Q., Cao, A. J., Sheng, H. W.** and **Ma, E.**, *Local order influences initiation of plastic flow in metallic glass: Effects of alloy composition and sample cooling history*, Acta Mater., Vol. 56, No. 18, pp. 5263, 2008.

[60] **Cheng, Y. Q., Cao, A. J.** and **Ma, E.**, *Correlation between the elastic modulus and the intrinsic plastic behavior of metallic glasses: The roles of atomic configuration and alloy composition*, Acta Mater., Vol. 57, No. 11, pp. 3253, 2009.

[61] **Miracle, D. B.**, *A structural model for metallic glasses*, Nat. Mater., Vol. 3, No. 10, pp. 697, 2004.

[62] **Bernal, J. D.**, *Geometrical approach to the structure of liquids*, Nature, Vol. 183, No. 4655, pp. 141, 1959.

[63] **Bernal, J. D.**, *Bakerian Lecture 1962 - Structure of liquids*, Proc. R. Soc. London, Ser. A, Vol. 280, No. 1380, pp. 299, 1964.

[64] **Scott, G. D.**, *Packing of equal spheres*, Nature, Vol. 188, No. 4754, pp. 908, 1960.

[65] **Scott, G. D.** and **Kilgour, D. M.**, *Density of random close packing of spheres*, J. Phys. D: Appl. Phys., Vol. 2, No. 6, pp. 863, 1969.

[66] **Finney, J. L.**, *Random packings and structure of simple liquids .1. Geometry of random Close Packing*, Proc. R. Soc. London, Ser. A, Vol. 319, No. 1539, pp. 479, 1970.

[67] **Voronoi, G. Z.**, *Nouvelles applications des parametres continus a la theorie des formes quadratiques.*, J. Reine u. Angew. Math., Vol. 134, pp. 199, 1908.

[68] **Brostow, W., Dussault, J. P.** and **Fox, B. L.**, *Construction Of Voronoi Polyhedra*, J. Comput. Phys., Vol. 29, No. 1, pp. 81, 1978.

[69] **Prins, J. A.** and **Petersen, H.**, *Theoretical diffraction patterns corresponding to some simple types of molecular arrangement in liquids*, Physica, Vol. 3, pp. 147, 1936.

[70] **Gaskell, P. H.**, *Structure of simple inorganic amorphous solids*, J. Phys. C: Solid State Phys., Vol. 12, No. 21, pp. 4337, 1979.

[71] **Gaskell, P. H.**, *Models for the structure of amorphous metals*, Top. Appl. Phys., p. 5, 1983.

[72] **Ma, D., Stoica, A. D.** and **Wang, X. L.**, *Power-law scaling and fractal nature of medium-range order in metallic glasses*, Nat. Mater., Vol. 8, No. 1, pp. 30, 2009.

[73] **Hirata, A., Guan, P. F., Fujita, T., Hirotsu, Y., Inoue, A., Yavari, A. R., Sakurai, T.** and **Chen, M. W.**, *Direct observation of local atomic order in a metallic glass*, Nat. Mater., Vol. 10, No. 1, pp. 28, 2011.

[74] **Sheng, H. W., Luo, W. K., Alamgir, F. M., Bai, J. M.** and **Ma, E.**, *Atomic packing and short-to-medium-range order in metallic glasses*, Nature, Vol. 439, No. 7075, pp. 419, 2006.

[75] **Miracle, D. B., Greer, A. L.** and **Kelton, K. F.**, *Icosahedral and dense random cluster packing in metallic glass structures*, J. Non-Cryst. Solids, Vol. 354, No. 34, pp. 4049, 2008.

[76] **Waseda, Y., Chen, H. S., Jacob, K. T.** and **Shibata, H.**, *On the glass forming ability of liquid alloys*, Sci. Technol. Adv. Mater., Vol. 9, No. 2, pp. 023003, 2008.

[77] **Schuh, C. A., Hufnagel, T. C.** and **Ramamurty, U.**, *Overview No.144 - Mechanical behavior of amorphous alloys*, Acta Mater., Vol. 55, No. 12, pp. 4067, 2007.

[78] **Spaepen, F.**, *Microscopic mechanism for steady-state inhomogeneous flow in metallic Glasses*, Acta. Metall., Vol. 25, No. 4, pp. 407, 1977.

[79] **Steif, P. S., Spaepen, F.** and **Hutchinson, J. W.**, *Strain localization in amorphous metals*, Acta. Metall., Vol. 30, No. 2, pp. 447, 1982.

[80] **Argon, A. S.**, *Plastic-deformation in metallic glasses*, Acta. Metall., Vol. 27, No. 1, pp. 47, 1979.

[81] **Spaepen, F.**, *Homogeneous flow of metallic glasses: A free volume perspective*, Scr. Mater., Vol. 54, No. 3, pp. 363, 2006.

[82] **Kobayashi, S., Maeda, K.** and **Takeuchi, S.**, *Computer-simulation of deformation of amorphous* $Cu_{57}Zr_{43}$, Acta. Metall., Vol. 28, No. 12, pp. 1641, 1980.

[83] **Srolovitz, D., Maeda, K., Vitek, V.** and **Egami, T.**, *Structural defects in amorphous solids statistical-analysis of a computer-model*, Philos. Mag. A: Phys. Condens. Matter Struct. Defects Mech. Prop., Vol. 44, No. 4, pp. 847, 1981.

[84] **Falk, M. L.** and **Langer, J. S.**, *Dynamics of viscoplastic deformation in amorphous solids*, Phys. Rev. E, Vol. 57, No. 6, pp. 7192, 1998.

[85] **Falk, M. L.** and **Maloney, C. E.**, *Simulating the mechanical response of amorphous solids using atomistic methods*, Eur. Phys. J. B, Vol. 75, No. 4, pp. 405, 2010.

[86] **Shi, Y. F.** and **Falk, M. L.**, *Atomic-scale simulations of strain localization in three-dimensional model amorphous solids*, Phys. Rev. B, Vol. 73, No. 21, pp. 214201, 2006.

[87] **Bailey, N. P., Schiotz, J.** and **Jacobsen, K. W.**, *Atomistic simulation study of the shear-band deformation mechanism in Mg-Cu metallic glasses*, Phys. Rev. B, Vol. 73, No. 6, pp. 064108, 2006.

[88] **Lee, J. C., Park, K. W., Kim, K. H., Fleury, E., Lee, B. J., Wakeda, M.** and **Shibutani, Y.**, *Origin of the plasticity in bulk amorphous alloys*, J. Mater. Res., Vol. 22, No. 11, pp. 3087, 2007.

[89] **Khonik, S. V., Granato, A. V., Joncich, D. M., Pompe, A.** and **Khonik, V. A.**, *Evidence of distributed interstitialcy-like relaxation of the shear modulus due to structural relaxation of metallic glasses*, Phys. Rev. Lett., Vol. 100, No. 6, pp. 065501, 2008.

[90] **Huang, R., Suo, Z., Prevost, J. H.** and **Nix, W. D.**, *Inhomogeneous deformation in metallic glasses*, J. Mech. Phys. Solids, Vol. 50, No. 5, pp. 1011, 2002.

[91] **Lu, J., Ravichandran, G.** and **Johnson, W. L.**, *Deformation behavior of the* $Zr_{41.2}Ti_{13.8}Cu_{12.5}Ni_{10}Be_{22.5}$ *bulk metallic glass over a wide range of strain-rates and temperatures*, Acta Mater., Vol. 51, No. 12, pp. 3429, 2003.

[92] **Allen, M. P.** and **Tldesley, D. J.**, Computer Simulation of Liquids, Oxford University Press, 1987.

[93] **Kohn, W.** and **Sham, L. J.**, *Self-consistent equations including exchange and correlation effects*, Phys. Rev., Vol. 140, No. 4A, pp. 1133, 1965.

[94] **Plimpton, S.**, *Fast parallel algorithms for short-range molecular dynamics*, J. Comput. Phys., Vol. 117, No. 1, pp. 1, 1995.

[95] **Nordlund, K.**, PARCAS Computer Code, 2007.

[96] **Guo, H., Yan, P. F., Wang, Y. B., Tan, J., Zhang, Z. F., Sui, M. L.** and **Ma, E.**, *Tensile ductility and necking of metallic glass*, Nat. Mater., Vol. 6, No. 10, pp. 735, 2007.

[97] **Abraham, F. F., Walkup, R., Gao, H. J., Duchaineau, M., De la Rubia, T. D.** and **Seager, M.**, *Simulating materials failure by using up to one billion atoms and the world's fastest computer: Work-hardening*, Proc. Natl. Acad. Sci. U. S. A., Vol. 99, No. 9, pp. 5783, 2002.

[98] **Jang, D. C.** and **Greer, J. R.**, *Transition from a strong-yet-brittle to a stronger-and-ductile state by size reduction of metallic glasses*, Nat. Mater., Vol. 9, No. 3, pp. 215, 2010.

[99] **Chen, C. Q., Pei, Y. T.** and **De Hosson, J. T. M.**, *Effects of size on the mechanical response of metallic glasses investigated through in situ TEM bending and compression experiments*, Acta Mater., Vol. 58, No. 1, pp. 189, 2010.

[100] **Mendelev, M. I., Sordelet, D. J.** and **Kramer, M. J.**, *Using atomistic computer simulations to analyze x-ray diffraction data from metallic glasses*, J. Appl. Phys., Vol. 102, No. 4, pp. 043501, 2007.

[101] **Tersoff, J.**, *Modeling solid-state chemistry: Interatomic potentials for multicomponent systems*, Phys. Rev. B, Vol. 39, No. 8, pp. 5566, 1989.

[102] **Berendsen, H. J. C., Postma, J. P. M., van Gunsteren, W. F., DiNola, A.** and **Haak, J. R.**, *Molecular dynamics with coupling to an external bath*, J. Chem. Phys., Vol. 81, No. 8, pp. 3684, 1984.

[103] **Shimizu, F., Ogata, S.** and **Li, J.**, *Theory of shear banding in metallic glasses and molecular dynamics calculations*, Mater. Trans., Vol. 48, No. 11, pp. 2923, 2007.

[104] **Stukowski, A.**, *Visualization and analysis of atomistic simulation data with OVITO-the Open Visualization Tool*, Modell. Simul. Mater. Sci. Eng., Vol. 18, No. 1, pp. 015012, 2010.

[105] **Li, J.**, *AtomEye: an efficient atomistic configuration viewer*, Modell. Simul. Mater. Sci. Eng., Vol. 11, No. 2, pp. 173, 2003.

[106] **Dickey, J. M.** and **Paskin, A.**, *Computer simulation of the lattice dynamics of solids*, Phys. Rev., Vol. 188, No. 3, pp. 1407, 1969.

[107] **Yu, R., Singh, D.** and **Krakauer, H.**, *All-electron and pseudopotential force calculations using the linearized-augmented-plane-wave method*, Phys. Rev. B, Vol. 43, No. 8, pp. 6411, 1991.

[108] **Wei, S.** and **Chou, M. Y.**, *Phonon dispersions of silicon and germanium from first-principles calculations*, Phys. Rev. B, Vol. 50, No. 4, pp. 2221, 1994.

[109] **Wang, H., Chu, W., Jin, H.** and **Xiong, Y.**, *Atomistic simulation of Si-Ge clathrate alloys*, Chem. Phys., Vol. 344, No. 3, pp. 299, 2008.

[110] **Porter, L. J., Justo, J. F.** and **Yip, S.**, *The importance of Gruneisen parameters in developing interatomic potentials*, J. Appl. Phys., Vol. 82, No. 11, pp. 5378, 1997.

[111] **Bording, J. K.** and **Tafto, J.**, *Molecular-dynamics simulation of growth of nanocrystals in an amorphous matrix*, Phys. Rev. B, Vol. 62, No. 12, pp. 8098, 2000.

[112] **Tsunekawa, S., Ishikawa, K., Li, Z. Q., Kawazoe, Y.** and **Kasuya, A.**, *Origin of anomalous lattice expansion in oxide nanoparticles*, Phys. Rev. Lett., Vol. 85, No. 16, pp. 3440, 2000.

[113] **Korotcov, A., Hsu, H. P., Huang, Y. S., Tsai, D. S.** and **Tiong, K. K.**, *Growth and characterization of well-aligned RuO_2 nanocrystals on oxide substrates via reactive sputtering*, Crystal Growth & Design, Vol. 6, No. 11, pp. 2501, 2006.

[114] **Groenen, J., Priester, C.** and **Carles, R.**, *Strain distribution and optical phonons in InAs/InP self-assembled quantum dots*, Phys. Rev. B, Vol. 60, No. 23, pp. 16013, 1999.

[115] **Shuttleworth, R.**, *The surface tension of solids*, Proc. Phys. Soc. London Sect. A, Vol. 63, No. 365, pp. 444, 1950.

[116] **Vermaak, J. S., Mays, C. W.** and **Kuhlmann.D**, *On surface stress and surface tension. Theoretical considerations*, Surf. Sci., Vol. 12, No. 2, pp. 128, 1968.

[117] **Shreiber, D.** and **Jesser, W. A.**, *Size dependence of lattice parameter for Si_xGe_{1-x} nanoparticles*, Surf. Sci., Vol. 600, No. 19, pp. 4584, 2006.

[118] **Faupel, F., Frank, W., Macht, M. P., Mehrer, H., Naundorf, V., Ratzke, K., Schober, H. R., Sharma, S. K.** and **Teichler, H.**, *Diffusion in metallic glasses and supercooled melts*, Rev. Mod. Phys., Vol. 75, No. 1, pp. 237, 2003.

[119] **Schober, H. R.**, *Collectivity of motion in undercooled liquids and amorphous solids*, J. Non-Cryst. Solids, Vol. 307, pp. 40, 2002.

[120] **Gibbs, J. H.** and **Dimarzio, E. A.**, *Nature of the glass transition and the glassy state*, J. Chem. Phys., Vol. 28, No. 3, pp. 373, 1958.

[121] **Okamoto, P. R., Lam, N. Q.** and **Rehn, L. E.**, *Physics of crystal-to-glass transformations*, Solid State Phys. - Adv. Res. Appl, Vol. 52, pp. 1, 1999.

[122] **Chen, H. S.**, Structural relaxation in metallic glasses, Butterworths, 1983.

[123] **Gerstein, M., Tsai, J.** and **Levitt, M.**, *The volume of atoms on the protein surface - calculated from simulation, using voronoi polyhedra*, J. Mol. Biol., Vol. 249, No. 5, pp. 955, 1995.

[124] **Kim, D. S., Chung, Y. C., Kim, J. J., Kim, D.** and **Yu, K.**, *Voronoi diagram as an analysis tool for spatial properties for ceramics*, J. Ceram. Process. Res., Vol. 3, No. 3, pp. 150, 2002.

[125] **Gellatly, B. J.** and **Finney, J. L.**, *Characterization of models of multicomponent amorphous metals - The radical alternative to the voronoi polyhedron*, J. Non-Cryst. Solids, Vol. 50, No. 3, pp. 313, 1982.

[126] **Takagi, T., Ohkubo, T., Hirotsu, Y., Murty, B. S., Hono, K.** and **Shindo, D.**, *Local structure of amorphous $Zr_{70}Pd_{30}$ alloy studied by electron diffraction*, Appl. Phys. Lett., Vol. 79, No. 4, pp. 485, 2001.

[127] **Cheng, Y. Q., Sheng, H. W.** and **Ma, E.**, *Relationship between structure, dynamics, and mechanical properties in metallic glass-forming alloys*, Phys. Rev. B, Vol. 78, No. 1, pp. 014207, 2008.

[128] **Wang, S., Kramer, M., Xu, M., Wu, S., Hao, S., Sordelet, D., Ho, K.** and **Wang, C.**, *Experimental and ab initio molecular dynamics simulation studies of liquid $Al_{60}Cu_{40}$ alloy*, Phys. Rev. B, Vol. 79, No. 14, pp. 144205, 2009.

[129] **Wendt, H. R.** and **Abraham, F. F.**, *Empirical Criterion for the Glass Transition Region Based on Monte Carlo Simulations*, Phys. Rev. Lett., Vol. 41, No. 18, pp. 1244, 1978.

[130] **Torquato, S.** and **Stillinger, F. H.**, *Controlling the short-range order and packing densities of many-particle systems*, J. Phys. Chem. B, Vol. 106, No. 33, pp. 8354, 2002.

[131] **Agoston, P.** and **Albe, K.**, *Formation entropies of intrinsic point defects in cubic In_2O_3 from first-principles density functional theory calculations*, Phys. Chem. Chem. Phys., Vol. 11, No. 17, pp. 3226, 2009.

[132] **Hao, S., Wang, C., Kramer, M.** and **Ho, K.**, *Microscopic origin of slow dynamics at the good glass forming composition range in $Zr_{1-x}Cu_x$ metallic liquids*, J. Appl. Phys., Vol. 107, No. 5, pp. 053511, 2010.

[133] **Jiang, W. H., Pinkerton, F. E.** and **Atzmon, M.**, *Mechanical behavior of shear bands and the effect of their relaxation in a rolled amorphous Al-based alloy*, Acta Mater., Vol. 53, No. 12, pp. 3469, 2005.

[134] **He, L., Zhong, M. B., Han, Z. H., Zhao, Q., Jiang, F.** and **Sun, J.**, *Orientation effect of pre-introduced shear bands in a bulk-metallic glass on its "work-ductilising"*, Mater. Sci. Eng., A, Vol. 496, No. 1-2, pp. 285, 2008.

[135] **Sutton, A.P. Balluffi, R.**, Interfaces in crystalline materials, Oxford Science Publications, Oxford, 1996.

[136] **Brostow, W., Chybicki, M., Laskowski, R.** and **Rybicki, J.**, *Voronoi polyhedra and Delaunay simplexes in the structural analysis of molecular-dynamics-simulated materials*, Phys. Rev. B, Vol. 57, No. 21, pp. 13448, 1998.

[137] **Kilo, M., Hund, M., Sauer, G., Baiker, A.** and **Wokaun, A.**, *Reaction induced surface segregation in amorphous CuZr, NiZr and PdZr alloys - An XPS*

and SIMS depth profiling study, J. Alloys Compd., Vol. 236, No. 1-2, pp. 137, 1996.

[138] **Bukowska, J., Kudelski, A.** and **JanikCzachor, M.**, *SERS on modified amorphous Cu-Zr alloys*, Chem. Phys. Lett., Vol. 268, No. 5-6, pp. 481, 1997.

[139] **Novakovic, R., Muolo, M. L.** and **Passerone, A.**, *Bulk and surface properties of liquid X-Zr (X = Ag, Cu) compound forming alloys*, Surf. Sci., Vol. 549, No. 3, pp. 281, 2004.

[140] **Yokoyama, Y.**, *Ductility improvement of Zr-Cu-Ni-Al glassy alloy*, J. Non-Cryst. Solids, Vol. 316, No. 1, pp. 104, 2003.

[141] **Zhang, J. L., Yu, H. B., Lu, J. X., Bai, H. Y.** and **Shek, C. H.**, *Enhancing plasticity of $Zr_{46.75}Ti_{8.25}Cu_{7.5}Ni_{10}Be_{27.5}$ bulk metallic glass by precompression*, Appl. Phys. Lett., Vol. 95, No. 7, pp. 071906, 2009.

[142] **Lund, A. C., Nieh, T. G.** and **Schuh, C. A.**, *Tension/compression strength asymmetry in a simulated nanocrystalline metal*, Phys. Rev. B, Vol. 69, No. 1, pp. 012101, 2004.

[143] **Sha, Z. D., Wu, R. Q., Lu, Y. H., Shen, L., Yang, M., Cai, Y. Q., Feng, Y. P.** and **Li, Y.**, *Glass forming abilities of binary $Cu_{100-x}Zr_x$ (x=34, 35.5, and 38.2 at. percent) metallic glasses: A LAMMPS study*, J. Appl. Phys., Vol. 105, No. 4, pp. 043521, 2009.

[144] **Salimon, A. I., Ashby, M. F., Brechet, Y.** and **Greer, A. L.**, *Bulk metallic glasses: what are they good for?*, Mater. Sci. Eng., A, Vol. 375, pp. 385, 2004.

[145] **Bruck, H. A., Christman, T., Rosakis, A. J.** and **Johnson, W. L.**, *Quasi-static constitutive behavior of $Zr_{41.25}Ti_{13.75}Ni_{10}Cu_{12.5}Be_{22.5}$ bulk amorphous-alloys*, Scr. Metall. Mater., Vol. 30, No. 4, pp. 429, 1994.

[146] **Fan, C.** and **Inoue, A.**, *Improvement of mechanical properties by precipitation of nanoscale compound particles in Zr-Cu-Pd-Al amorphous alloys*, Mater. Trans., JIM, Vol. 38, No. 12, pp. 1040, 1997.

[147] **Petch, N. J.**, *The cleavage strength of polycrystals*, Journal of the Iron and Steel Institute, Vol. 174, No. 1, pp. 25, 1953.

[148] **Pauly, S., Gorantla, S., Wang, G., Kuhn, U.** and **Eckert, J.**, *Transformation-mediated ductility in CuZr-based bulk metallic glasses*, Nat. Mater., Vol. 9, No. 6, pp. 473, 2010.

[149] **Valentin, A., See, J., Galdin-Retailleau, S.** and **Dollfus, P.**, *Study of phonon modes in silicon nanocrystals using the adiabatic bond charge model*, J. Phys.: Condens. Matter, Vol. 20, No. 14, pp. 145213, 2008.

[150] **Richter, H., Wang, Z. P.** and **Ley, L.**, *The one phonon Raman spectrum in microcrystalline silicon*, Solid State Commun., Vol. 39, No. 5, pp. 625, 1981.

[151] **Pizzagalli, L., Galli, G., Klepeis, J. E.** and **Gygi, F.**, *Structure and stability of germanium nanoparticles*, Phys. Rev. B, Vol. 63, No. 16, pp. 165324, 2001.

[152] **Hudon, C., Meyer, R.** and **Lewis, L. J.**, *Low-frequency vibrational properties of nanocrystalline materials: Molecular dynamics simulations of two-dimensional systems*, Phys. Rev. B: Condens. Matter, Vol. 76, No. 4, pp. 045409, 2007.

[153] **Gupta, S. K.** and **Jha, P. K.**, *Modified phonon confinement model for size dependent Raman shift and linewidth of silicon nanocrystals*, Solid State Commun., Vol. 149, No. 45-46, pp. 1989, 2009.

[154] **Nien, Y.-T., Zaman, B., Ouyang, J., Chen, I.-G., Hwang, C.-S.** and **Yu, K.**, *Raman scattering for the size of CdSe and CdS nanocrystals and comparison with other techniques*, Mater. Lett., Vol. 62, No. 30, pp. 4522, 2008.

[155] **Chuu, D. S., Dai, C. M., Hsieh, W. F.** and **Tsai, C. T.**, *Raman investigations of the surface modes of the crystallites in CdS thin films grown by pulsed laser and thermal evaporation*, J. Appl. Phys., Vol. 69, No. 12, pp. 8402, 1991.

[156] **Mykhaylyk, O. O., Solonin, Y. M., Batchelder, D. N.** and **Brydson, R.**, *Transformation of nanodiamond into carbon onions: A comparative study by high-resolution transmission electron microscopy, electron energy-loss spectroscopy, x-ray diffraction, small-angle x-ray scattering, and ultraviolet Raman spectroscopy*, J. Appl. Phys., Vol. 97, No. 7, pp. 074302, 2005.

[157] **Weber, T. A.** and **Stillinger, F. H.**, *Local order and structural transitions in amorphous metal-metalloid Alloys*, Phys. Rev. B, Vol. 31, No. 4, pp. 1954, 1985.

[158] **Honeycutt, J. D.** and **Andersen, H. C.**, *Molecular dynamics study of melting and freezing of small Lennard-Jones clusters*, J. Phys. Chem., Vol. 91, No. 19, pp. 4950, 1987.

[159] **Wallace, D. C.**, Thermodynamics of Crystals, Dover Publications, 31 East 2nd Street, Mineola, N.Y. 11501, 1998.

[160] **Yamakov, V., Wolf, D., Phillpot, S. R.** and **Gleiter, H.**, *Grain-boundary diffusion creep in nanocrystalline palladium by molecular-dynamics simulation*, Acta Mater., Vol. 50, No. 1, pp. 61, 2002.

[161] **Nieh, T.** and **Wadsworth, J.**, *Hall-petch relation in nanocrystalline solids*, Scr. Metall. Mater., Vol. 25, No. 4, pp. 955, 1991.

[162] **Araujo, L. L., Giulian, R., Sprouster, D. J., Schnohr, C. S., Llewellyn, D. J., Kluth, P., Cookson, D. J., Foran, G. J.** and **Ridgway, M. C.**, *Size-dependent characterization of embedded Ge nanocrystals: Structural and thermal properties*, Phys. Rev. B, Vol. 78, No. 9, pp. 094112, 2008.

[163] **Sopu, D., Albe, K., Ritter, Y.** and **Gleiter, H.**, *From nanoglasses to bulk massive glasses*, Appl. Phys. Lett., Vol. 94, No. 19, pp. 191911, 2009.

[164] **Ghafari, M., Sopu, D., Brand, R., Mattheis, R., Kruk, R., Albe, K., Hahn, H.** and **Kamli, S.**, *Stabilization of amorphous transition metal layer in Fe/a-CoFeB multilayers*, Submitted.

[165] **Gleiter, H.**, *Our thoughts are ours, their ends none of our own: Are there ways to synthesize materials beyond the limitations of today?*, Acta Mater., Vol. 56, No. 19, pp. 5875, 2008.

[166] **Durukanoglu, S., Kara, A.** and **Rahman, T. S.**, *Local and excess vibrational free energies of stepped metal surfaces*, Phys. Rev. B, Vol. 67, No. 23, pp. 235405, 2003.

[167] **Wang, Y. M., Li, J., Hamza, A. V.** and **Barbee, T. W.**, *Ductile crystal line-amorphous nanolaminates*, Proceedings of the National Academy of Sciences of the United States of America, Vol. 104, No. 27, pp. 1115, 2007.